

pubs.acs.org/JCTC Article

# Graph-IQ\(Cl), a Graph-Based Quantum/Classical Algorithm for Efficient Electronic Structure on Hybrid Quantum/Classical Hardware Systems: Improved Quantum Circuit Depth Performance

Juncheng Harry Zhang and Srinivasan S. Iyengar\*



Cite This: https://doi.org/10.1021/acs.jctc.1c01303



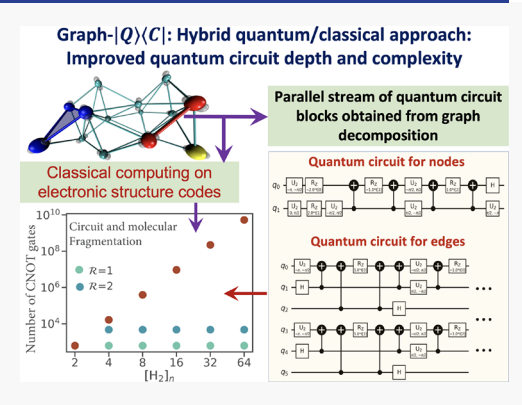
ACCESS

Metrics & More

Article Recommendations

Supporting Information

**ABSTRACT:** We present a procedure to reduce the depth of quantum circuits and improve the accuracy of results in computing post-Hartree—Fock electronic structure energies in large molecular systems. The method is based on molecular fragmentation where a molecular system is divided into overlapping fragments through a graph-theoretic procedure. This allows us to create a set of projection operators that decompose the unitary evolution of the full system into separate sets of processes, some of which can be treated on quantum hardware and others on classical hardware. Thus, we develop a procedure for an electronic structure that can be asynchronously spawned onto a potentially large ensemble of classical and quantum hardware systems. We demonstrate this method by computing Unitary Coupled Cluster Singles and Doubles (UCCSD) energies for a set of  $[H_2]_n$  clusters, with n ranging from 4 to 128. We implement our methodology using quantum circuits, and when these quantum circuits are processed on a



quantum simulator, we obtain energies in agreement with the UCCSD energies in the milli-hartree energy range. We also show that our circuit decomposition approach yields up to 9 orders of magnitude reduction in the number of CNOT gates and quantum circuit depth for the large-sized clusters when compared to a standard quantum circuit implementation available on IBM's Quantum Information Science kit, known as Qiskit.

#### 1. INTRODUCTION

Computing accurate electronic properties, including the effect of electron correlation and nuclear dynamics, is at the heart of modern quantum chemistry, with potential impact on materials discovery, 1-3 and the accurate study of biological 4-10 and atmospheric 11-13 processes. However, such studies are deeply confounded by (a) the steep (algebraic) computational scaling of accurate electron correlation methods, <sup>14–16</sup> where, for example, the gold standard of electronic structure theory, namely, CCSD(T), scales as  $O(N^{6-7})$  and (b) the likely exponential scaling of quantum nuclear dynamics. Over the years, several classical algorithms have been developed to improve the computational scaling of both problems. 17-21 For example, molecular fragmentation has recently become a critical tool to compute electronic properties and has grown to provide extremely accurate and effective computational paradigms. Similarly, the effect of nuclear dynamics has also been an active area of study for complex reactive processes. 22-24

Recently, multiple quantum computing technologies, such as ion traps, <sup>26–29</sup> superconducting coils, <sup>30,31</sup> Bosonic processors with photons, <sup>32–34</sup> solid-state devices and quantum dots inside cavities, <sup>35–38</sup> and Rydberg atoms, <sup>39–41</sup> have emerged as potential alternative computational platforms to address complex computational challenges. Additionally, algorithms to approximate electron correlation problems, <sup>42–63</sup> for small

molecular systems, and quantum nuclear dynamics problems<sup>64-71</sup> have been implemented on quantum hardware devices using trapped atomic ions, photons, nuclear spins, quantum dots, Rydberg atoms, and superconducting circuits. However, as outlined in Figure 1, application of standard quantum circuit models<sup>25</sup> to treat electronic structure problems leads to a rapid increase in the circuit depth and the number of CNOT gates. This contributes greatly to the accumulated error during quantum propagation. Quantum gate fidelity for CNOT gates is generally of the order of 95%, 72 and the improvement of such gate fidelity is an active area of quantum hardware development.<sup>73</sup> This is related to the fact that the CNOT gates require maximally entangling  $XX(\pi/2)$  gates and hence have lower-quality performance<sup>72</sup> as compared to small-angle XX gates, and this aspect contributes to error propagation. As seen in Figure 1, the number of quantum gates, the number of CNOT gates, and the circuit depth increase exponentially with system size. This leads to a dramatic increase in the error in quantum

Received: December 25, 2021



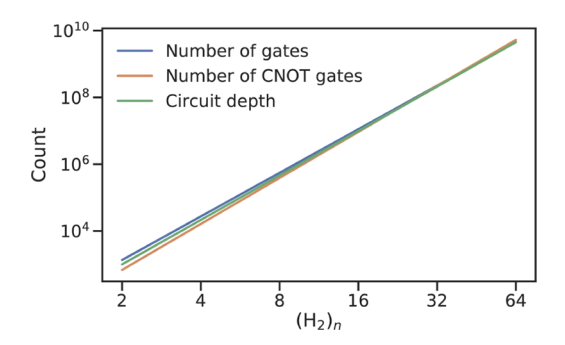


**Figure 1.** Quantum circuit depth complexity as a function of system size is illustrated here for a family of  $(H_2)_n$  clusters. As the system size grows, a standard quantum circuit implementation afforded by the commonly used Qiskit<sup>25</sup> quantum computing model becomes prohibitively complex.

propagation thus restricting both the size and quality (in terms of basis set sizes that can be routinely used) of performance. Thus, despite the growing set of available quantum hardware platforms and the accompanying set of complex quantum algorithms, performing accurate, state-of-the-art quantum chemical calculations will remain a significant challenge for the foreseeable future. In this publication, we present a new hybrid quantum/classical algorithm that helps reduce the number of CNOT gates, the circuit depth, and the total number of gates by several orders of magnitude. This paper outlines a new hybrid algorithm based on a graph-theoretic approach to molecular fragmentation and is geared toward performing electron correlation calculations, potentially on an ensemble of quantum and classical hardware systems. From here on, the algorithm studied here is referred to as the "Graph- $|Q\rangle\langle C|$ " algorithm since it contains an independent set of classical and quantum algorithmic components inside a single umbrella. That is, the overall computational workload is partitioned, through graph theory based on computational complexity analysis, into (a) classical computing sections that are carried out on traditional classical electronic structure packages, such as Gaussian,<sup>7</sup> Psi4,<sup>75</sup> ORCA,<sup>76</sup> and Quantum ESPRESSO,<sup>77</sup> and (b) quantum computing sections that are carried out using quantum circuit models. Furthermore, the Graph- $|Q\rangle\langle C|$  algorithm is quantum hardware-agnostic and is developed with the goal to be implemented on all quantum hardware technologies, and, in fact, is designed to be used on an ensemble of such quantum hardware systems for any given calculation. In essence, our Graph- $|Q\rangle\langle C|$  algorithm yields a new approach that reduces the required quantum circuit depth, the number of quantum gates, and the number of CNOT gates (by several orders of magnitude) that contribute to error accumulation (the scaling of these three properties is shown in Figure 1), through a graphtheory-based projection operator formalism. Thus, given this reduction, our algorithm, which is complementary to other ideas in the literature \$33,59-61,63 that attempt to reduce quantum gate complexity, potentially improves the quantum algorithmic efficiency, provides a new avenue for quantum resource management, and also reduces the accumulation of errors during the demonstrated electronic structure calculations on quantum hardware. Given the limitations of quantum circuit gate fidelities within the gate model, this algorithm, which we expect, will become a central piece in the quantum/classical computing of chemical systems.

Our approach begins with a graph-theoretic molecular fragmentation procedure introduced in refs 22, 23, and 78-

85, where the key idea begins with the well-known ONIOM methodology; 86 however, then, the "model" and "real" system energies and gradients within ONIOM are now constructed using many-body expansions up to an arbitrary rank. Furthermore, these many-body expansions are obtained in a general fashion using adaptive graph-theoretic techniques that are computationally available within standard protocols in the Python programing language. This paper is organized as follows: in Sections 2 and 3, we outline our graph-theoretic molecular fragmentation approach and also describe how these are to be implemented within a hybrid ensemble of quantum and classical hardware systems to yield reduced complexity of quantum circuits. We show that the graph-theoretic approach yields a unitary transformation applied to the quantum circuit model corresponding to the full quantum molecular system to reduce it into a family of decoupled, parallel quantum circuit models, each of which has much lower complexity as compared to the parent circuit. Thus, we expect that the error propagation in this new family of circuits is far less as compared to that belonging to the parent full system. In Section 4, we demonstrate the reduction in quantum circuit complexity scaling that arises from our algorithm through results for hydrogen molecular clusters. Conclusions are given in Section 5.

## 2. GRAPHICAL REPRESENTATION OF LOCAL MANY-BODY INTERACTIONS MAPPED TO OUANTUM CIRCUIT MODELS

Thus far, the electronic structure of small systems 42-46,50,87 or low-classical scaling approximations of the same for larger systems<sup>52</sup> have been implemented on quantum technologies. Here, we develop an approach, based on graph-theoretic fragmentation of molecular systems, that provides a pathway toward an accurate depiction of electron correlation on large systems using hybrid quantum/classical algorithms appropriate for an ensemble of quantum and classical computing environments. In a series of publications, <sup>22,23,78–85</sup> we have developed graph theory-based techniques to compute efficient and adaptive many-body expansions that are then embedded within the ONIOM<sup>86</sup> multi-layer approach; the accuracy and efficiency of these methods have been demonstrated on classical hardware systems. In this paper, we develop algorithms that make this approach applicable to a hybrid set of quantum and classical hardware systems. The salient features of this approach are as follows: the molecular assembly is partitioned into a set of nodes or vertices. Generally, these nodes are determined on a chemical basis and may include groups such as water and hydronium <sup>22,23,83,85</sup> or a single amino acid group in a poly-peptide chain. 81,82 These nodes are used to provide approximations to local molecular 1-body electronic energy contributions. Firstorder interactions between these discrete nodes are captured by creating edges, that are the union of two nodes. Once the nodes and edges are defined, the chemical system of interest is now represented as a graph. (An illustration of our graph-theoretic partitioning of the molecular structure is presented in Figure 2.) Higher-order (or *n*-body) terms can then be considered based upon the connectivity of the nodes, and the criteria to determine this connectivity have been discussed in detail in refs 81 and 83. As the rank or order of the terms increases, the graph-theoretic fragmentation approximation rapidly converges toward accurate electron correlation energies for single-geometry calculations and during ab initio molecular dynamics simulations but at progressively increasing computation cost.

Article

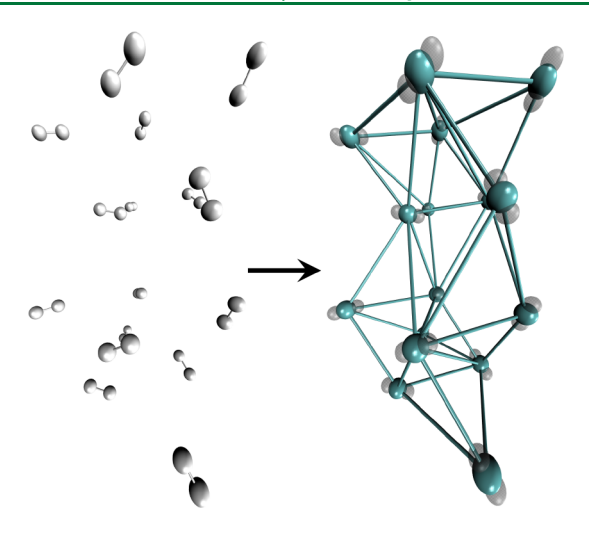


**Figure 2.** Here, a cluster of 16 hydrogen molecules is represented as a graph. This graph presents a distance-based truncation of expensive electron correlation treatments. This graphical representation also allows for the reduction in complexity for the quantum circuit representation of this system s discussed later in this paper.

In the discussion below, the set of nodes described above is represented as  $V_0$ . Similarly, the set edges that represent the set of first-order interactions between nodes are represented as  $V_1$ . Together, these nodes and edges define a graph,  $\mathcal{G} \equiv \{V_0; V_1\}$  (see Figure 2). The graph, thus, comprises nodes,  $V_0$ , edges,  $V_1$ , and rank-r simplexes, represented as  $V_r$ , that capture higher-order interactions between the nodes and is given by

$$\{\mathbf{V}_{\mathbf{r}}|r=0, 1, 2, ...\} \equiv \{\mathbf{V}_{\mathbf{0}}, \mathbf{V}_{\mathbf{1}}, \mathbf{V}_{\mathbf{2}}, ...\}$$
 (1)

The above presented graphical description allows a dynamic and flexible representation of local many-body interactions. The energetic measure we begin with \$^{22,23,78-85}\$ consists of a perturbative, ONIOM-type correction to a result obtained at a lower level of theory, where the perturbative correction is the difference between two many-body expansions (replacing the standard "model-high" minus "model-low" portion in ONIOM) given by the graphical representation presented above. Consistent with the notions behind ONIOM, \$^{86}\$ we have \$^{22,78-85}\$ an energy expression

$$E_{\rm MBE,gt}^{\rm ONIOM}(\overline{\mathbf{x}}) = E^{\rm level,0}(\overline{\mathbf{x}}) + E_{\rm MBE}^{\rm level,1}(\overline{\mathbf{x}}) - E_{\rm MBE}^{\rm level,0}(\overline{\mathbf{x}}) \tag{2}$$

where the left side,  $E_{\rm MBE,gt}^{\rm ONIOM}(\overline{\mathbf{x}})$ , denotes the graph-theoretically obtained many-body correction to ONIOM, and the term  $E_{\rm MBE}^{\rm level,I}(\overline{\mathbf{x}})$  on the right side may encompass the full system or a chosen "active site", and we have considered both options within AIMD<sup>78–82,85</sup> and quantum nuclear potential surface treatments. <sup>22,23</sup> In addition to the extrapolatory, ONIOM-like form of eq 2, each term in the extrapolation is a many-body expansion, that is now written in a general and computationally robust fashion up to order (or rank)  $\mathcal R$  as

$$E_{\text{MBE}}^{\text{level,I}} = \sum_{r=0}^{\mathcal{R}} (-1)^r \sum_{\alpha \in \mathbf{V_r}} E_{\alpha,r}^{\text{level,I}} \left[ \sum_{m=r}^{\mathcal{R}} (-1)^m p_{\alpha}^{r,m} \right]$$

$$= \sum_{r=0}^{\mathcal{R}} (-1)^r \sum_{\alpha \in \mathbf{V_r}} E_{\alpha,r}^{\text{level,I}} \mathcal{M}_{\alpha}^r$$
(3)

where  $p_{\alpha}^{r,m}$  is the number of times the  $\alpha$ th (r+1)-body term (in set  $V_r$ ) appears in all (m+1)-body terms (in set  $V_m$  for  $m \ge r$ ),

and consequently,  $\mathcal{M}_{\alpha}^{r} \equiv \left[\sum_{m=r}^{\mathcal{R}} (-1)^{m} p_{\alpha}^{r,m}\right]$  is the overcounting correction for the number of times the  $\alpha$ th (r+1)-body term appears in all objects of rank greater than or equal to r. It is important to emphasize that eq 3 is essentially identical to standard many-body expressions but presented now using graph theory. Thus, the full energy expression, which combines eqs 2 and 3, becomes

$$E_{\text{MBE,gt}}^{\text{ONIOM}} = E^{\text{level,0}} + \sum_{r=0}^{\mathcal{R}} (-1)^r \left\{ \sum_{\alpha \in \mathbf{V_r}} (E_{\alpha,r}^{\text{level,1}} - E_{\alpha,r}^{\text{level,0}}) \mathcal{M}_{\alpha}^r \right\}$$
$$= E^{\text{level,0}} + \Delta \text{MBE}_{\mathcal{R}}^{\text{level,1};\text{level,0}}$$
(4)

In practice, the individual simplexes in eqs 3 and 4 are computed independently and asynchronously, <sup>85</sup> leading to a general Python-based parallel implementation. Furthermore, our implementation also allows use of separate electronic structure packages for each level of treatment and currently supports the simultaneous use of Gaussian, <sup>74</sup> ORCA, <sup>76</sup> Psi4, <sup>75</sup> Quantum ESPRESSO, <sup>77</sup> and OpenMX. <sup>88</sup> A few key ideas regarding our graph-theoretic formalism are presented in the Supporting Information to facilitate the discussion in the paper.

### 3. GRAPH-THEORETICALLY DETERMINED PARALLEL QUANTUM CIRCUITS FROM EQS 3 AND 4

As seen in the Introduction section, the problem of quantum circuit depth is a serious limitation in obtaining accurate quantum computing results. In this section, we present a general solution to this problem based on the graph-theoretic paradigm presented in the previous section. The graphical decomposition of the instantaneous molecular structure is parsed, and the steep scaling aspects (represented as "level, 1" in eq 4) are spawned to a quantum computing or quantum simulation system, while the lower scaling components are retained on classical hardware. To achieve this, in Section 3.1, we develop a general projection operator-based formalism, which when applied to a full-system molecular quantum circuit, as shown in in Section 3.2, reduces the circuit into a family of parallel quantum circuits. In the Results and Discussion section, we have then shown that this approach reduces the quantum circuit depth problem, shown in Figure 1, by several orders of magnitude.

**3.1. Graph-Theory-Based Projection Operators.** In this section, we introduce a new quantum circuit decomposition technique that reduces the complexity of circuits (measured in terms of circuit depth and number of CNOT gates as seen in Figure 1) by several orders of magnitude. We begin with a Hilbert space decomposition scheme using the set-theoretic inclusion—exclusion principle. <sup>89</sup> The projection technique is then adapted to a graph problem, which in the next subsection is used to decompose any arbitrary unitary operator (or quantum circuit) into parallel, but overlapping, streams of computing processes that can be executed on a cluster of quantum and classical hardware systems.

Let us begin with a Venn diagram that divides a coordinate representation  $|x\rangle\langle x|$  into regions, A, B, C, and so forth. The regions may intersect, and in Figure 3a, for concreteness, we have superimposed the Venn diagram on top of a  $H_2$  molecular cluster. Thus, the Venn divides a molecular system into several regions. Using the principle of inclusion and exclusion, <sup>89</sup> the resolution of the identity for the Hilbert space depicted within the Venn diagram may be written as

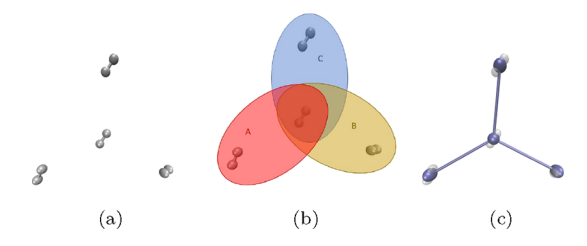


**Figure 3.** In figure (b), we provide an illustration of the sets A, B, and C for the system in figure (a). Figure (b) is used to construct eq 5. In figure (c), the sets are provided a graph-theoretic form to make the transition from eq 5 to 7 clear. Figure (c) can be realized through eq 9 which is a special case of eq 7.

$$\mathbf{I} \equiv \int_{A \cup B \cup C} dx |x\rangle \langle x|$$

$$= \int_{A} dx |x\rangle \langle x| + \int_{B} dx |x\rangle \langle x| + \int_{C} dx |x\rangle \langle x|$$

$$- \int_{A \cap B} dx |x\rangle \langle x| - \int_{A \cap C} dx |x\rangle \langle x| - \int_{B \cap C} dx |x\rangle \langle x|$$

$$+ \int_{A \cap B \cap C} dx |x\rangle \langle x|$$

$$= \mathcal{P}_{A} + \mathcal{P}_{B} + \mathcal{P}_{C} - \mathcal{P}_{A \cap B} - \mathcal{P}_{A \cap C} - \mathcal{P}_{B \cap C} + \mathcal{P}_{A \cap B \cap C}$$
(5)

where the left side is the identity since it sums over the entire Hilbert space represented here by sets A, B, and C, and integrals involving the dyadic terms,  $|x\rangle\langle x|$ , are within a chosen set depicted within the Venn diagram. Additionally, we have also introduced projection operators

$$\mathcal{P}_{A} \equiv \int_{A} \mathrm{d}x \, |x\rangle\langle x| \tag{6}$$

that project out portions of a Hilbert space depicted in eq 5 and only include the portion of the diadic sum within a given set.

While eq 5 arises from the principle of inclusion and exclusion<sup>89</sup> well known in set theory and can be generalized to

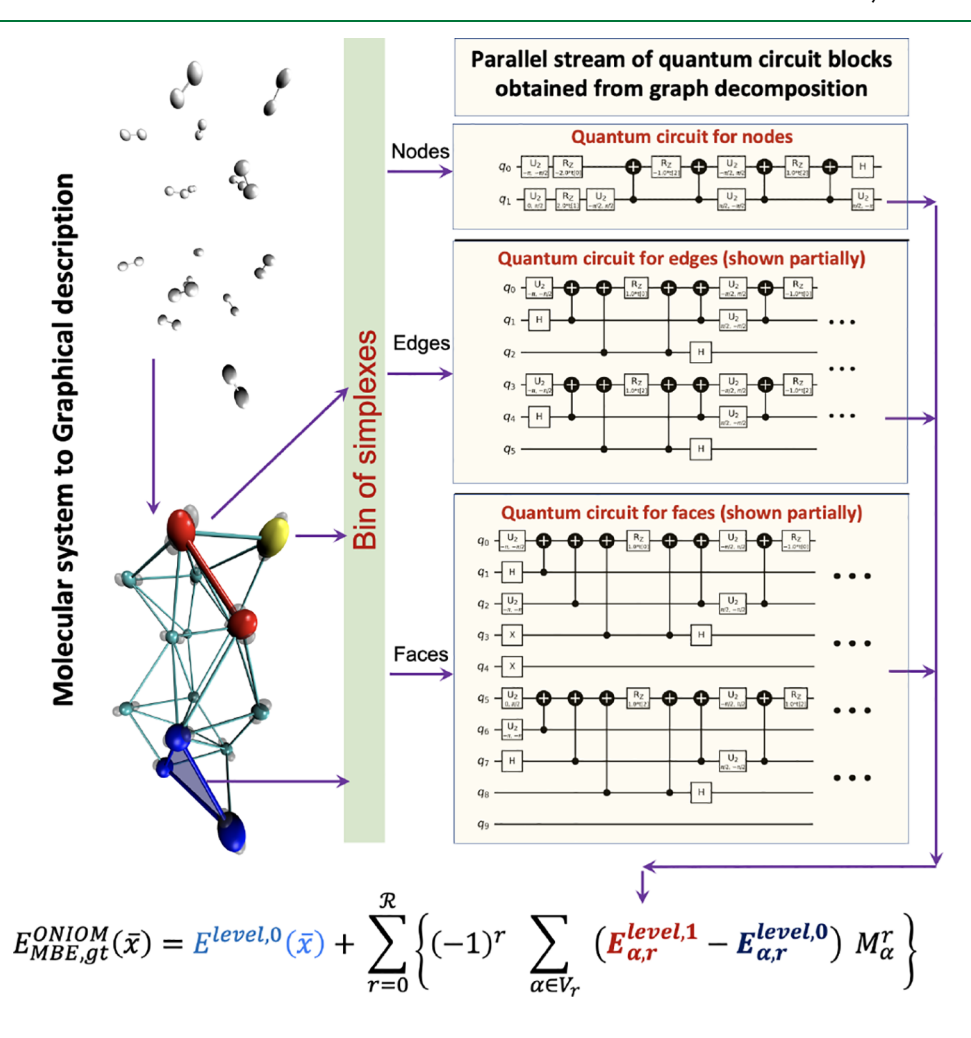


**Figure 4.** Quantum circuit decomposition based on graphical partitioning of molecular systems. The second-quantized Hamiltonians for node/edge/face fragments, with molecular orbitals obtained from Hartree—Fock, are used as the input for the Qiskit quantum computing framework, <sup>25</sup> to obtain quantum circuit models shown on the right side of the figure, one circuit for each fragment. Details of this process are given in the Results and Discussion section.

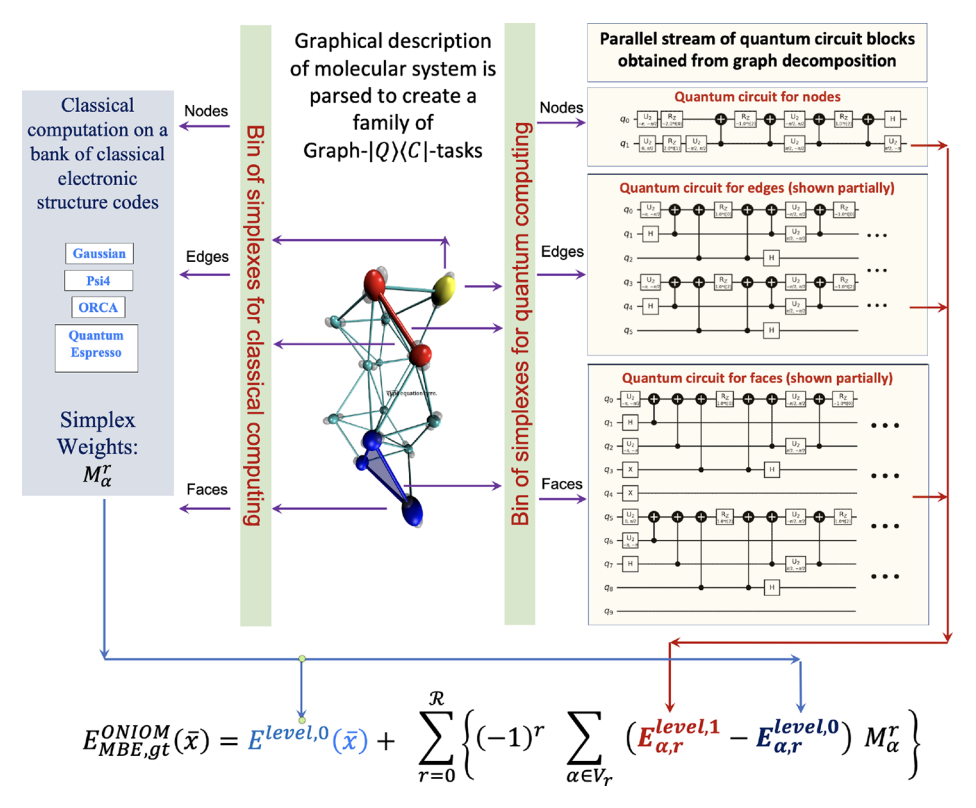


Figure 5. Figure 4 presents a quantum circuit decomposition based on graphical partitioning of molecular systems. This helps compute  $\{E_{a,r}^{\text{level},1}\}$  in eq 4. To compute the lower-scaling  $\{E_{a,r}^{\text{level},0}\}$ , we use classical computing algorithms as seen on the left side of the figure here.

an arbitrary number of sets, an alternate approach to divide the space represented by the identity operator, I, can be obtained by reintroducing the graph  $\mathcal{G} \equiv \{V_0; V_1\}$  from the previous section (also see Figure 2). As usual, the graph comprises vertices,  $V_0$ , edges,  $V_1$ , and rank-r simplexes. An equivalent expression for the resolution of the identity in eq 5 may now be obtained in terms of projectors that encompass nodes, edges, and higher-order simplexes as

$$\mathbf{I} = \sum_{\alpha \in \mathbf{V_0}} \mathcal{M}_{\alpha}^0 \mathcal{P}_{\alpha,0} - \sum_{\alpha \in \mathbf{V_1}} \mathcal{M}_{\alpha}^1 \mathcal{P}_{\alpha,1} + \sum_{\alpha \in \mathbf{V_2}} \mathcal{M}_{\alpha}^2 \mathcal{P}_{\alpha,2} - \dots$$

$$= \sum_{r=0}^{\mathcal{R}} (-1)^r \sum_{\alpha \in \mathbf{V_r}} \mathcal{M}_{\alpha}^r \mathcal{P}_{\alpha,r}$$
(7)

Here, as in eqs 3 and 4,  $\mathcal{M}_{\alpha}^{r} \equiv \left[\sum_{m=r}^{\mathcal{R}} (-1)^{m} p_{\alpha}^{r,m}\right]$  and  $p_{\alpha}^{r,m}$  are the number of times the  $\alpha$ th rank-r term (in set  $\mathbf{V}_{\mathbf{r}}$ ) appears in all rank-m terms (in set  $\mathbf{V}_{\mathbf{m}}$ ), for  $m \geq r$ . Consequently,  $\mathcal{M}_{\alpha}^{r}$  is the overcounting correction for the number of times the  $\alpha$ th rank-r term appears in all objects of a rank greater than or equal to r. It must be noted that  $p_{\alpha}^{r,m}$  are also the number of supersets of the  $\alpha$ th rank-r simplex, and the projectors,  $\mathcal{P}_{\alpha,r}$ , yield the  $\alpha$ -th rank-r simplex. These projection operators are used in the next section to reduce the quantum circuit depth.

The parallels between eqs 7 and 5 may be further explored by rewriting eq 7 in a decreasing order of rank, that is

$$\mathbf{I} = (-1)^{\mathcal{R}} \left\{ \sum_{\alpha \in \mathbf{V}_{\mathcal{R}}} \mathcal{P}_{\alpha,\mathcal{R}} - \sum_{\alpha \in \mathbf{V}_{\mathcal{R}-1}} \mathcal{M}_{\alpha}^{\mathcal{R}-1} \mathcal{P}_{\alpha,\mathcal{R}-1} + \sum_{\alpha \in \mathbf{V}_{\mathcal{R}-2}} \mathcal{M}_{\alpha}^{\mathcal{R}-2} \mathcal{P}_{\alpha,\mathcal{R}-2} - \sum_{\alpha \in \mathbf{V}_{\mathcal{R}-3}} \mathcal{M}_{\alpha}^{\mathcal{R}-3} \mathcal{P}_{\alpha,\mathcal{R}-3} + \ldots \right\}$$
(8)

where the appearance of alternating signs is clear and resembles that in eq 5, and the factor  $\mathcal{M}_{\alpha}^{\mathcal{R}-1}$  is the number of times the  $\alpha$ -th rank- $(\mathcal{R}-1)$  simplex appears in all rank- $\mathcal{R}$  simplexes. Additionally, for  $\mathcal{R}=1$ , eq 8 becomes

$$\mathbf{I} = -\sum_{\alpha \in \mathbf{V}_{1}} \mathcal{P}_{\alpha,1} + \sum_{\alpha \in \mathbf{V}_{0}} \mathcal{M}_{\alpha}^{0} \mathcal{P}_{\alpha,0}$$
(9)

which, for the graph in Figure 3c, leads to an identical result as in eq 5, constructed for Figure 3b.

**3.2.** Quantum Circuit Depth Reduction through Parallel Quantum Processing Using the Projection Operators,  $\{\mathcal{P}_{\alpha,r}\}$ . We now begin with a quantum circuit depicted using the symbol  $\mathcal{U}$ , a unitary operator, that propagates a state that represents the electronic structure for the full molecular system on some quantum hardware system. However, as noted in Figure 1, the complexity of such a circuit and the associated resources may grow rapidly as system size grows. To overcome this issue, we may apply the graph-theoretically defined resolution of identity in eq 7 to  $\mathcal{U}$  to decompose it into a family of parallel quantum circuits given by

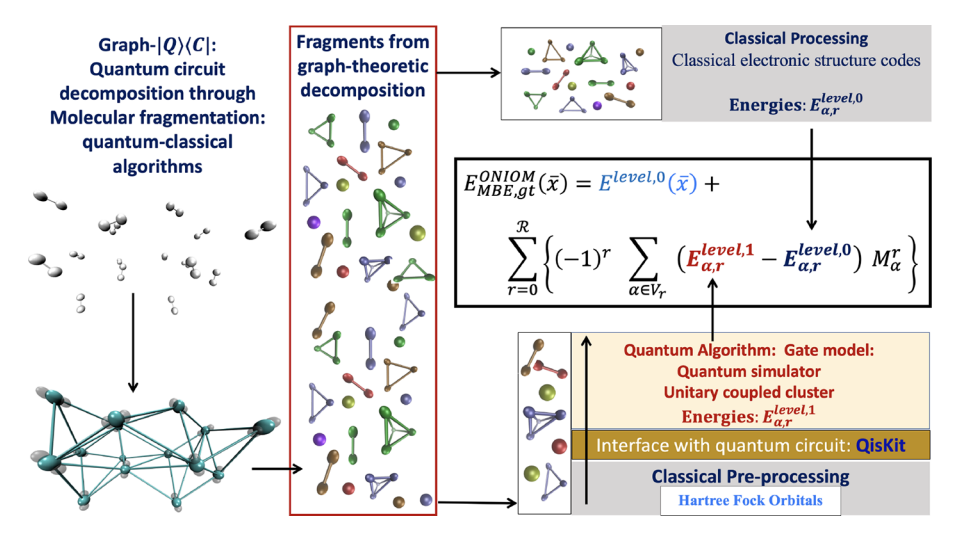


Figure 6. The algorithm has classical as well as quantum counterparts. See also Figure 5.

$$\mathbf{I}\mathcal{U} = \sum_{r=0}^{\mathcal{R}} (-1)^r \sum_{\alpha \in \mathbf{V_r}} \mathcal{M}_{\alpha}^r [\mathcal{P}_{\alpha,r} \mathcal{U}]$$
$$= \sum_{r=0}^{\mathcal{R}} (-1)^r \sum_{\alpha \in \mathbf{V_r}} \mathcal{M}_{\alpha}^r \mathcal{U}_{\alpha,r}$$
(10)

where

$$\{\mathcal{U}_{\alpha,r} \equiv \mathcal{P}_{\alpha,r}\mathcal{U}\}\tag{11}$$

represents here a set of projected quantum circuits, one for each simplex. When a molecular system is divided using the graph, as presented in Section 2, the set  $\{\mathcal{U}_{\alpha,r}\}$  yields one quantum circuit for each molecular fragment. This is illustrated in Figure 4. Thus, using eq 10, it is possible to independently construct the unitary quantum circuits,  $\mathcal{U}_{\alpha,r}$ , one for each molecular fragment and use these in parallel on a family of decoupled quantum hardware systems to perform the computations needed to obtain the approximations in eqs 3 and 4.

In this publication, we use the individual quantum circuits,  $\{\mathcal{U}_{\alpha,r}\}$ , to obtain the family of fragment energies  $\{E_{\alpha,r}^{\text{level},1}\}$ , using quantum circuit models, where level, 1 here is Unitary Coupled Cluster Singles and Doubles (UCCSD), which when used in eq 10, or equivalently, eq 3, yields an approach to compute the left side of eq 4, using a stream of parallel quantum processes. This idea is presented in Figure 4. Because these independent circuits,  $\{\mathcal{U}_{\alpha,r}\}$ , are for much smaller fragments as compared to the full system of interest, one may find the error propagation to be limited. We indeed find this to be the case for the examples discussed later.

Furthermore, eq 4 contains both level, 1 calculations and level, 0 calculations. This kind of composite approach has been shown to converge faster as a function of maximum rank- $\mathcal{R}^{83,85}$  for ground-state post-Hartree–Fock energies, AIMD trajectories, and multi-dimensional potential calculations using post-Hartree–Fock energies and gradients. Here, level, 1 is UCCSD, whereas level, 0 will include a computationally less expensive DFT approximations. Thus, the algorithm presented here envisions spawning out a family of processes on an ensemble of classical and quantum systems, and this process is depicted in Figure 5 and, in more detail, in Figure 6.

It is critical to emphasize at this stage that it is now accepted 90,91 that universal, fully fault-tolerant quantum

computers are a rather distant dream, 90 and new frontiers such as Noisy Intermediate-Scale Quantum (NISQ) 90 systems have emerged. To effectively use such NISQ machines with their limited coherence times, a hybrid approach that interleaves NISQ machines with classical computers has been proposed in ref 91. This is complemented by orthogonal developments in quantum chemical algorithm developments where the variational quantum eigensolver (VQE) 62,63 is already known to be a hybrid quantum/classical approach. In this regard, our approach here, containing quantum and classical algorithmic components, is a contribution that can be used for ground-state quantum chemical calculations at enhanced accuracy with lower computational complexity 80-83,85 on a hybrid stream of quantum and classical systems. The algorithm is built to be asynchronous and parallel, and these computational aspects will be considered in a future publication.

In general, a molecular system, and in future a molecular surface,  $^{83}$  is coarse-grained to create a graphical representation as explained at the top of Section 2. This yields simplexes that are then used to create a "bucket of fragments" as referred to in Figures 4 and 5. Each fragment needs to be used to compute energies at two levels of theory,  $E_{\alpha,r}^{\rm level,1}$  and  $E_{\alpha,r}^{\rm level,0}$ . As stated in Figure 5, the quantity  $E_{\alpha,r}^{\rm level,0}$  is computed on classical hardware systems, whereas the quantity  $E_{\alpha,r}^{\rm level,1}$  is to be computed on quantum hardware using the quantum circuits  $\mathcal{U}_{\alpha,r}$ , as facilitated by the graph-theoretic partitioning method, thus expanding the realm of applications for quantum computation. In this publication, we do not present results that use actual quantum hardware, but we present results where the family of quantum circuits,  $\{\mathcal{U}_{\alpha,r}\}$ , is processed using the Qiskit system but implemented on a quantum simulator. Further computational details are presented in Section 4.1.

#### 4. RESULTS AND DISCUSSION

In order to gauge the accuracy and reduction in computational complexity arising from our Graph- $|Q\rangle\langle C|$  method presented above, we have applied this approach to a range of hydrogen molecular cluster problems. These systems are critical for applications related to energy storage. In particular, the safe and efficient storage 95,97–100 of molecular hydrogen is of paramount importance to potential developments in new fuel cell technologies. Furthermore, the study of orthoand para-hydrogen at low-temperatures has been a funda-

mental challenge that has implications toward the study of exotic new states of matter that may have important applications in low-temperature physics.  $^{110-112}$ 

While the key properties of such systems involve the detailed study of electronic as well as nuclear degrees of freedom, <sup>113</sup> in this publication, our goal is to gauge the accuracy of the approach introduced above the ability to reduce the complexity of quantum circuits in obtaining post-Hartree–Fock (coupled cluster)-level electronic energies for such systems. Thus, we compute post-Hartree–Fock electronic energies using the quantum circuit decomposition algorithm mentioned above and compare these results with those obtained using classical algorithms<sup>74,75</sup> obtained at the unitary coupled cluster level of theory (UCCSD).

Hydrogen molecular clusters of various sizes,  $(H_2)_m$ , (n=2,...,128) have been treated with the Graph- $|Q\rangle\langle C|$  method to demonstrate scalability and accuracy as the system size grows. Specifically, the analysis of errors due to the truncation in the rank  $(\mathcal{R} \text{ in eq } 10)$  and edge length cutoff used in the graph definition allows us to gauge the fragment circuit complexity needed to achieve an acceptable (milli-hartree) level of accuracy.

**4.1. Computational Aspects.** Figure 5 provides a brief overview of the algorithm which is further elaborated upon in Figure 6. Specifically, simplexes labeled  $(\alpha, r)$ , in eqs 10 and 4, are pre-determined on classical hardware. Each hydrogen molecule is treated as a node in the graph. The process of defining a graph is controlled by two parameters, the maximum edge length cutoff and the maximum order (or rank) of the many-body terms which is represented in eqs 10 and 4 using the symbol  $\mathcal{R}$ . As the maximum edge length increases, the fragments (including higher-order simplexes) grow in number and size rapidly, thus increasing computational complexity while also presenting a significant challenge for parallel processing. The edge length cutoff may be chosen to be high enough to include all critical interactions. The maximum edge length has been chosen here based on previous studies, 81,85 as well as additional analysis presented in the next subsection, and leads to the type of graph presented in Figures 4 and 5.

Once the graph is generated, the system is decomposed into a set of simplexes, or fragments, that essentially now can be processed in a completely independent way. A stream of fragments is thus generated with the goal to compute  $\{E^{\text{level},1}(\alpha,$ r);  $E^{\text{level},0}(\alpha,r)$ } and  $E^{\text{level},0}$  for the full system. As discussed in ref 85, the stream of fragments generated can be processed in an asynchronous (non-blocking) and parallel manner, to generate the fragment energies  $E^{\rm level,0}$  and  $E^{\rm level,1}$ , to be used in eq 4. In refs 83 and 85, this is done through an MPI parallelized hybrid C+ +/Python module, which is capable of using multiple electronic structure packages within a single AIMD step and isolated electronic structure calculations conducted during potential surface evaluations.<sup>22</sup> The implementation of the approach in classical computing platforms currently supports the following set of external electronic structure packages during a single energy and gradient evaluation: Gaussian,<sup>74</sup> ORCA,<sup>76</sup> and for molecular and cluster calculations, and Quantum ESPRESSO<sup>77</sup> and OpenMX<sup>88</sup> for condensed phase studies. Here, this aspect is further expanded to also include the use of quantum algorithms to determine  $E^{\text{level},1}$ . (See Figures 5 and 6.)

All level, 0 calculations shown in eq 4 were performed at the level of DFT (B3LYP), using a classical algorithm on classical hardware, and all level, 1 calculations were performed at the UCCSD level of theory, on a quantum simulator using an appropriate quantum circuit model. This choice of comple-

mentary levels of theory has been demonstrated to be accurate  $^{79,80,85}$  and to yield a rapidly convergent sequence of results this increasing graphical rank  $\mathcal{R}$ . The choice of basis sets for all calculations in this publication is limited to the minimal STO-3G since a larger basis set introduces more Hartree–Fock orbitals, which are mapped to an even greater number of excitation operators, thus significantly increasing the number of qubits required as well as the associated quantum circuit depth. While our approach will address all of these challenges, by reducing the needed circuit depth, in this publication, we probe the principle behind our execution model for accuracy purposes. Furthermore, as we will see later, it is straightforward to integrate the current scheme into other circuit optimization techniques, to further increase the size of systems that can be studied, and this will be considered as a part of future publications.

The following steps are used to obtain  $\{E^{\text{level},1}(\alpha, r)\}$  with quantum algorithms:

- 1. Hartree—Fock orbitals for each molecular fragment are classically pre-computed to create a family of second-quantized Fermionic Hamiltonians, and these are together provided as input to the Qiskit quantum computing framework, <sup>25</sup> as shown on the bottom-right portion of Figure 6.
- 2. The family of fragment second-quantized Fermionic Hamiltonians is then converted into quantum circuits,  $\{\mathcal{U}_{\alpha,r}\}$ , using a parity mapping protocol. 114
- 3. Each fragment quantum circuit is then executed on the Qiskit's built-in state vector simulator without using a noise model, and the resultant energies are optimized using the SLSQP optimizer<sup>115</sup> available within the VQE.<sup>50</sup> This yields the family of UCCSD energies,  $\{E^{\text{level},1}(\alpha,r)\}$ , used to obtain the molecular energy as per eq 4.

The following comments are in order with respect to the steps mentioned above. The hybrid quantum/classical formalism developed here is transparent to the underlying quantum mapping protocol used to convert the Fermionic Hamiltonians for each individual molecular fragment into quantum circuits. Thus, there are no restrictions on the kind of map used to treat each individual fragment Hamiltonian, and in principle, we can use the Jordan–Wigner, <sup>116</sup> Bravyi–Kitaev, <sup>117</sup> or parity mapping <sup>114</sup> transformations. Here, we have tested the Jordan–Wigner scheme as well as the parity mapping protocol, and we found that the latter does in fact reduce the qubit resources needed as suggested in ref 114. Specifically, for each quantum circuit, two qubits are reduced with the spin-parity symmetries of the system, <sup>114</sup> as a separate optimization technique.

There have been several recent studies that allow the implementation of variational quantum algorithms such as the VQE,  $^{42,43,50,51,53,87}$  in combination with an appropriate trial wavefunction such as the UCC ansatz  $^{118,119}$  on quantum simulation systems. However, our approach is general enough to allow the possibility to include other eigensolvers apart from the VQE, such as the recently developed contracted quantum eigensolver  $^{120}$  to compute the set of  $\{E^{\mathrm{level},1}(\alpha,r)\}$  values from the associated two-particle reduced density matrices. These aspects will be further investigated in future publications.

**4.2.** Reduction of Circuit Depth and Associated Accuracy. The complexity of our algorithm is determined by the maximum value of  $\mathcal{R}$  within the family of quantum circuits:  $\{\mathcal{U}_{\alpha,r}\}_{r=0}^{r}$ . Furthermore, these graph-based circuit complex-

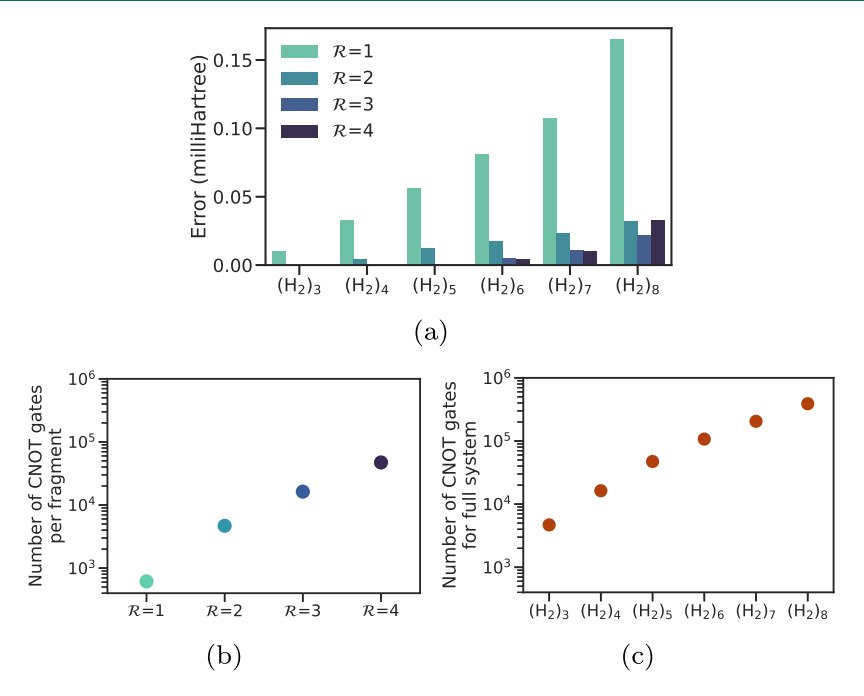


Figure 7. Results for the fully connected graph where the edge length has been chosen to be the maximum value so that all nodes are connected. (a) Errors from the Graph- $|Q\rangle\langle C|$  method at various values of  $\mathcal{R}$  in eq 10, as compared to the full UCCSD result. (b) Corresponding maximum quantum circuit depth requirement as a function of rank. As the maximum rank of the graph increases, the quantum circuit complexity increases in a near-exponential fashion. (c) Quantum circuit depth for the full system without the Graph- $|Q\rangle\langle C|$  treatment. For example, for  $(H_2)_8$ , the number of CNOT gates and associated circuit depth reduce from approximately  $10^6$  to approximately  $10^4$ , when  $\mathcal{R}=2$  is used while resulting in an error less than 0.05 milli-hartree.

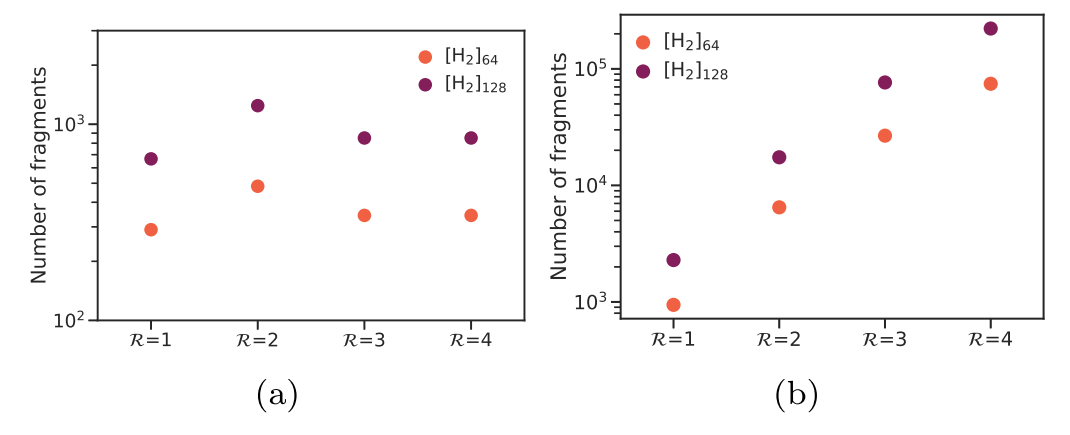
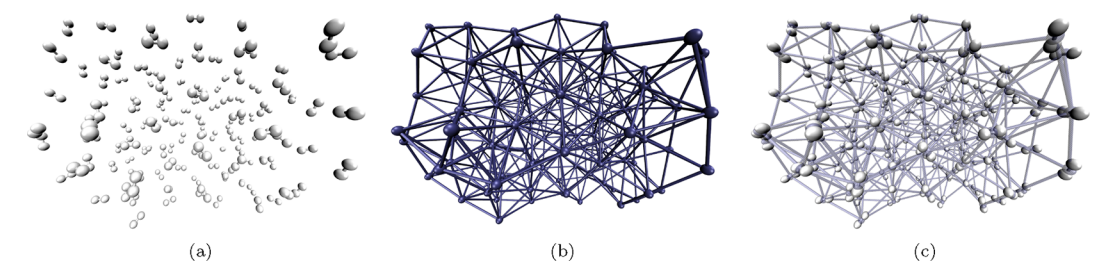


Figure 8. Number of fragment circuits for  $[H_2]_{64}$  and  $[H_2]_{128}$  at maximum edge lengths of 4 (a) and 7.5 Å (b) and various values of  $\mathcal{R}$ .

ities are also dictated by the maximum edge length that is used to create the graphs. Thus, we first conducted a detailed analysis of the accuracy of our algorithm when both the maximum edge length as well as  ${\mathcal R}$  are varied and chosen to have values up to their respective maximum possible values. We perform this analysis for systems in the size range  $[H_2]_n$ , n = 1, ..., 8, and present our results in Figure 7. For comparison, we provide results where quantum circuits are used for  $\{\mathcal{U}_{\alpha,r}|_{r=0...R}\}$  within the algorithm described above and depicted in Figure 6 and when classical algorithms are used to compute the  $\{E^{\text{level},1}(\alpha,r)\}$ energies. For all these cases, the maximum edge length is chosen such that all nodes are connected, that is, completely connected graphs are used, and the rank is progressively increased to study the accuracy as well as the efficiency in Figure 7. For all cases, given the similarity of the behavior of the three measures depicted in Figure 1, namely, the number of quantum gates, the number of CNOT gates, and the circuit depth, and given the

sensitivity of CNOT gate fidelity as discussed in ref 46, for the remaining portion of this paper, we use the number of CNOT gates within a quantum circuit as a measure of computational complexity and extent of error propagation.

As noted in Figure 7a, for each system shown along the horizontal axis, the accuracy increases as the maximum rank is increased and is already within 1/100th of a milli-hartree from the correct result at  $\mathcal{R}=2$ . In fact, for all cases in Figure 7a,  $\mathcal{R}=1$  provides results with acceptable accuracy. In Figure 7b, we present the computational effort needed to obtain the results in Figure 7a. That is, the larger rank calculations need an exponentially greater number of CNOT gates, which is a measurement of computational complexity, as seen in Figure 1. However, Figure 7b should be compared with Figure 7c, where the full-system computational complexity (or CNOT gate count) is presented. The number of CNOT gates in 7c is several orders of magnitude greater as compared to the truncated  $\mathcal R$ 



**Figure 9.** Complements Figure 8 and shows the drastically increasing number of fragments with increasing  $\mathcal{R}$ . (a)  $[H_2]_{128}$ . (b) Graphical decomposition of  $[H_2]_{128}$ , where each  $H_2$  molecule is treated as a node, and edges connect all nodes within a 4.0 Å distance. (See also Figure 10 and associated discussion on the edge length cutoff.) (c) Merged atomic and graphical images.

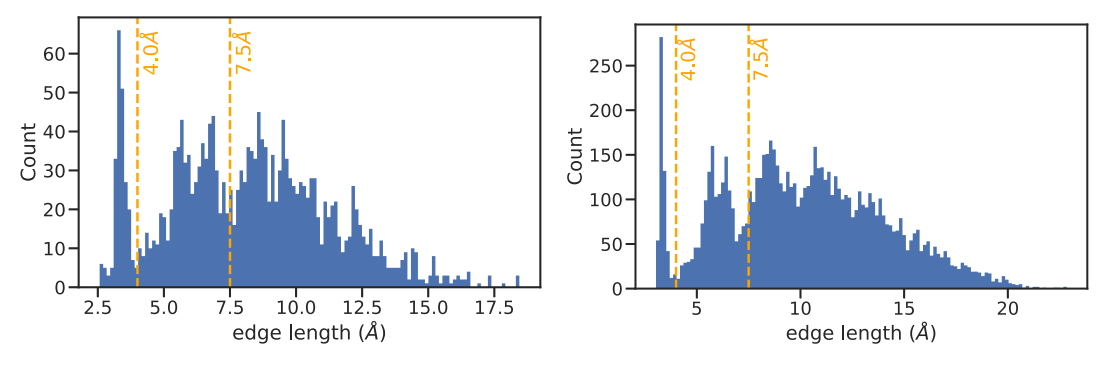
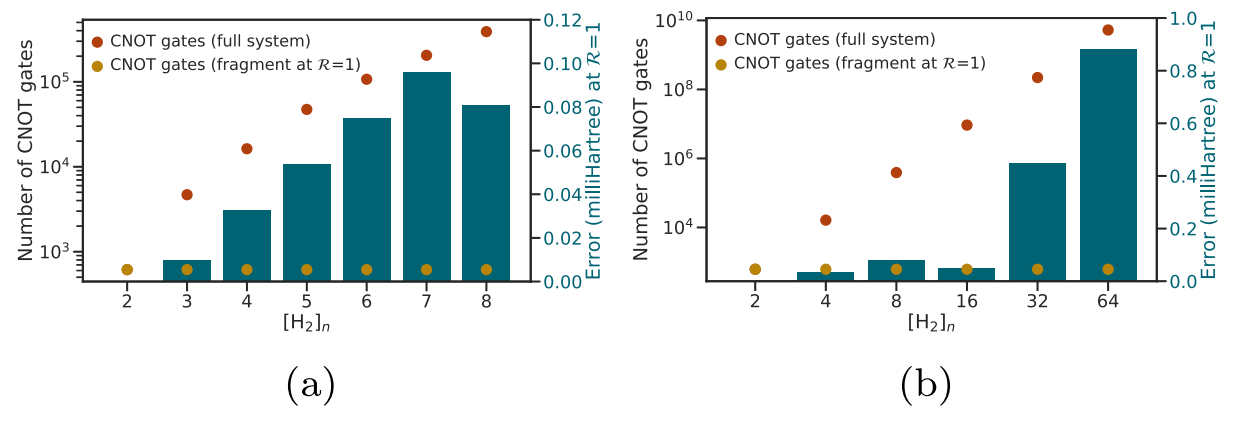


**Figure 10.** Radial distribution function for  $[H_2]_{64}$  and  $[H_2]_{128}$ .



ı

**Figure 11.** Results for larger  $H_2$  clusters. (a,b) 4.0 Å and  $\mathcal{R} = 1$ .

-level calculations in Figure 7b; for example, using only  $\mathcal{R}=1$  results in a 1-3 orders of magnitude reduction in the number of CNOT gates, as seen by comparison of Figure 7b,c, while maintaining accuracy to within 0.15 milli-hartree. Furthermore, the complexity for a specific choice of rank  $\mathcal{R}$ , which is dictated by an expected accuracy for the result as shown in Figure 7a, is constant across systems of all sizes. For example, for  $[H_2]_8$  at  $\mathcal{R}=1$ , instead of computing all interactions with the full system circuit, only 1-body and 2-body interactions are accounted for by a set of circuits representing  $[H_2]$  and  $[H_2]_2$ . The approximation takes advantage of the local nature of chemical systems.

However, there are some caveats. The computational expense of an individual fragment circuit increases with increasing values of  $\mathcal{R}$ , as seen in Figure 7b. In addition, as shown in Figure 8 and illustrated in Figure 9 for  $[H_2]_{128}$ , the number of fragment circuits also drastically escalates with respect to  $\mathcal{R}$ . Thus, the benefit of complexity (or the CNOT count) reduction from using fragments will also require the stream of quantum and

classical computations to be executed in parallel to attain computational efficiency.

In this publication, we aim to achieve a milli-hartree-level agreement between full UCCSD calculations and those obtained from the algorithms presented here. Thus, based on our results in Figure 7a, we now investigate larger  $[H_2]_n$  clusters, with n=8, ..., 128, using  $\mathcal{R}=1$  as the maximum rank. The maximum edge length for these larger clusters was determined based on the distribution of all edge lengths presented in Figure 10. This figure indicates that a maximum edge length of 4.0 Å includes most of the short-range interactions. Additional longer-range interactions may also be included by raising the maximum edge length to 7.5 Å; however, as stated above, the number of simplexes grows rapidly as the edge length increases thus raising the complexity of the algorithm.

The set of results for larger  $H_2$  clusters is presented in Figures 11 and 12. While Figure 11a summarizes the results for  $[H_2]_n$  clusters, with n = 1, ..., 8, Figure 11b extends this out to  $[H_2]_{64}$ . As the size of the molecular system grows, the corresponding

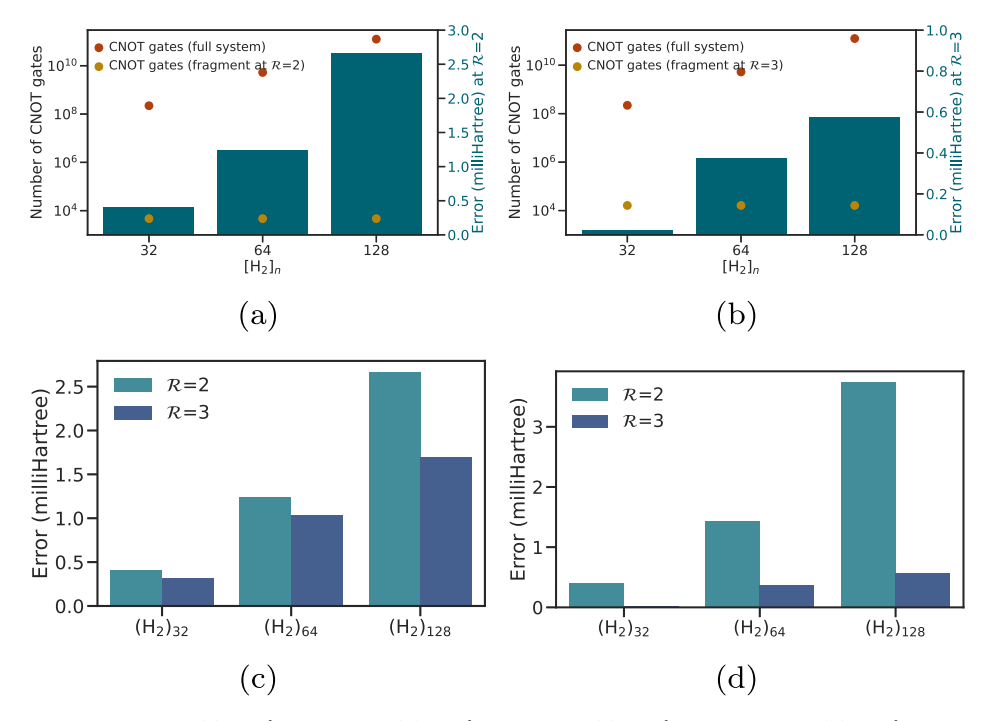


Figure 12. Results for larger  $H_2$  clusters. (a) 4.0 Å and  $\mathcal{R} = 2$ . (b) 7.5 Å and  $\mathcal{R} = 3$ . (c) 4.0 Å and  $\mathcal{R} = 2$ , 3. (d) 7.5 Å and  $\mathcal{R} = 2$ , 3. These figures show the progressive improvement in accuracy [(c,d)] and the associated increase in costs [see the relative vertical position of yellow dots in (a,b)].

circuit complexity, as represented by the number of CNOT gates (red dots), increases exponentially. However, the complexity of the current algorithm, as represented by the yellow dots in Figure 11, grows in a gradual fashion while maintaining accuracy in the milli-hartree range as can be seen from the right vertical axis of Figure 11. Clearly, these figures also show that while  $\mathcal{R}=1$  appears sufficient and does provide accurate results, the error grows with system size. Thus, in Figure 12a,b, we present the accuracy and CNOT gate count for  $\mathcal{R}=2$  and  $\mathcal{R}=3$ . Clearly, increasing the value of  $\mathcal{R}$  not only reduces the error but also increases the number of CNOT gates as seen in Figure 12c,d.

A more complete picture for circuit complexity can be seen from Table 1, where we present the circuit depth, the number of qubits, the number of CNOT gates, the total number of gates, and the number of parameters needed to describe a quantum circuit, using the standard implementation available in Qiskit,

Table 1. Quantum Circuit Resource Requirements When Standard Techniques Are Used: Illustration for a Family of H<sub>2</sub> Clusters<sup>a</sup>

system	circuit depth	number of qubits	number of CNOT gates	total number of gates	number of parameters
$H_2$	11	2	3	16	3
$(H_2)_2$	924	6	615	1217	26
$(H_2)_3$	5920	10	4684	7370	117
$(H_2)_4$	21 361	14	16 285	27 021	360
$(H_2)_5$	57 402	18	47 312	70 204	875
$(H_2)_6$	128 469	22	107 190	156 081	1818
$(H_2)_7$	253 846	26	205 192	313 143	3381
$(H_2)_8$	458 233	30	389 472	550 279	5792

"Clearly, as the system size grows, the circuit gets extremely complex. The Graph-IQ\⟨Cl approach reduces resource complexity by several orders of magnitude.

for clusters of various sizes. Thus, as per Figure 11, when  $\mathcal{R}=1$  is used for these calculations, the resources needed are as dictated by the second row (i.e.,  $[H_2]_2$ ) in Table 1. This provides a significant reduction in the resources needed to perform these computations, as noted in the figures mentioned above.

Thus, in general, choice of maximum  $\mathcal{R}$  and edge length cutoff would be based on a compromise between the desired accuracy and efficiency. However, in all cases, it appears that the current algorithm presents a powerful mode to reduce the quantum circuit depth problem in quantum computing, as summarized by Figure 13.

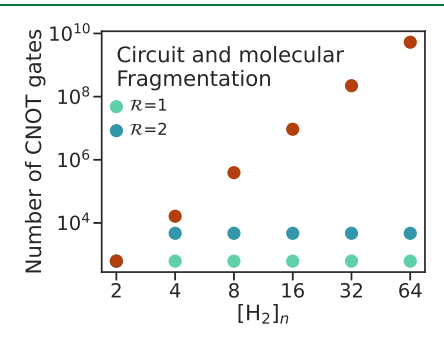


**Figure 13.** Summary of reduction in CNOT gate-based complexity. The red circles are the standard implementation, whereas the blue and green circles arise from the circuit decomposition scheme discussed here.

#### 5. CONCLUSIONS

The promise of solving exponentially complex problems efficiently using quantum computing hardware and associated quantum computing algorithms software is a rapidly evolving research frontier. While we are in the early stages of this quantum revolution, there are a wide set of scientific and technological areas that can benefit from such developments.

However, true progress in such areas can only be achieved by a rigorous study and understanding of the electronic structure and dynamics of complex materials, thus requiring accurate treatment of electron correlation effects in conjunction with a rigorous treatment of quantum nuclear effects.

Many groups have contributed greatly to the development of new quantum circuit-based methodologies to compute the electronic structure in small molecular systems on quantum hardware. Most of these efforts are deeply hindered by the so-called quantum circuit depth problem where the complexity of the quantum circuit, along with the limited fidelity of the quantum gates currently available on state-of-the-art quantum hardware, leads to an enormous increase in error propagation and in stable implementation. This provides a strong upper bound on the accuracy, system size, and levels of basis functions that can be implemented in currently available quantum hardware.

In this publication, we present a novel procedure to reduce the depth of quantum circuits and reduce the extent to which this influences the quality of results in computing post-Hartree—Fock electronic structure energies. The method is based on molecular fragmentation, and specifically, a molecular system is divided into overlapping fragments through a graph-theoretic technique. This then allows the construction of a series of projection operators, that allow some overall model for quantum computing obtained from an approximation to the unitary evolution of the full system, into separate processes, some of which can be treated on quantum hardware and others on classical hardware. Thus, we develop a procedure for electronic structure that can be spawned on to a potentially large ensemble of classical and quantum hardware systems.

We demonstrate this methodology by computing UCCSD energies for a set of  $[H_2]_n$  clusters, with n ranging from 4 to 128. We implement our methodology using quantum circuits, and when these quantum circuits are processed on a quantum simulator, we obtain energies in agreement with the correct UCCSD energies in the milli-hartree energy range. We also show that our circuit decomposition approach yields up to 9 orders of magnitude reduction in the number of CNOT gates and circuit depth for the larger-sized clusters when compared to a standard quantum circuit implementation as available within Qiskit. Future work will involve the implementation of these methods on quantum hardware.

#### ASSOCIATED CONTENT

#### **Solution** Supporting Information

The Supporting Information is available free of charge at https://pubs.acs.org/doi/10.1021/acs.jctc.1c01303.

A few key ideas regarding our graph-theoretic formalism including the generation of nodes, edges, and the definition of higher-order ( $\mathcal{R}$ -rank) simplexes that capture  $\mathcal{R}-1$ -body interactions in the molecular system as per eqs 4 and 10 (PDF)

#### AUTHOR INFORMATION

#### **Corresponding Author**

Srinivasan S. Iyengar — Department of Chemistry and Department of Physics, Indiana University, Bloomington, Indiana 47405, United States; orcid.org/0000-0001-6526-2907; Email: iyengar@indiana.edu

#### **Author**

Juncheng Harry Zhang — Department of Chemistry and Department of Physics, Indiana University, Bloomington, Indiana 47405, United States

Complete contact information is available at: https://pubs.acs.org/10.1021/acs.jctc.1c01303

pubs.acs.org/JCTC

#### Notes

The authors declare no competing financial interest.

#### ACKNOWLEDGMENTS

This research was supported by the National Science Foundation grants CHE-2102610 and OMA-1936353 to author S.S.I. Author J.H.Z. was awarded a Lee J. Todd Chemistry Scholarship from the Indiana University Department of Chemistry to support his summer undergraduate research.

#### REFERENCES

- (1) Iannuzzi, M.; Parrinello, M. Proton Transfer in Heterocycle Crystals. *Phys. Rev. Lett.* **2004**, 93, 025901.
- (2) Tse, Y.-L. S.; Herring, A. M.; Kim, K.; Voth, G. A. Molecular dynamics simulations of proton transport in 3M and nafion perfluorosulfonic acid membranes. *J. Phys. Chem. C* **2013**, *117*, 8079.
- (3) Lin, I.-H.; Lu, Y.-H.; Chen, H.-T. Nitrogen-doped  $C_{60}$  as a robust catalyst for CO oxidation. *J. Comput. Chem.* **2017**, 38, 2041–2046.
- (4) Field, M. J.; Bash, P. A.; Karplus, M. A Combined Quantum Mechanical and Molecular Mechanical Potential for Molecular Dynamics Simulations. *J. Comput. Chem.* **1990**, *11*, 700.
- (5) Wong, K.-Y.; Gao, J. Insight into the phosphodiesterase mechanism from combined QM/MM free energy simulations. *FEBS J.* **2011**, *278*, 2579–2595.
- (6) Harris, D. L. Oxidation and Electronic State Dependence of Proton Transfer in the Enzymatic Cycle of Cytochrome P450eryF. *J. Inorg. Biochem.* **2002**, *91*, 568.
- (7) Lin, Y.-l.; Gao, J. Kinetic Isotope Effects of L-Dopa Decarboxylase. *J. Am. Chem. Soc.* **2011**, *133*, 4398.
- (8) Rega, N.; Iyengar, S. S.; Voth, G. A.; Schlegel, H. B.; Vreven, T.; Frisch, M. J. Hybrid Ab-Initio/Empirical Molecular Dynamics: Combining the ONIOM Scheme with the Atom-Centered Density Matrix Propagation (ADMP) Approach. J. Phys. Chem. B 2004, 108, 4210.
- (9) Iyengar, S. S.; Sumner, I.; Jakowski, J. Hydrogen Tunneling in an Enzyme Active Site: A Quantum Wavepacket Dynamical Perspective. *J. Phys. Chem. B* **2008**, *112*, 7601.
- (10) Phatak, P.; Sumner, I.; Iyengar, S. S. Gauging the Flexibility of the Active Site in Soybean Lipoxygenase-1 (SLO-1) Through an Atom-Centered Density Matrix Propagation (ADMP) Treatment That Facilitates the Sampling of Rare Events. J. Phys. Chem. B 2012, 116, 10145
- (11) Gerber, R. B.; Sebek, J. Dynamics Simulations of Atmospherically Relevant Molecular Reactions. *Int. Rev. Phys. Chem.* **2009**, 28, 207.
- (12) Dietrick, S. M.; Pacheco, A. B.; Phatak, P.; Stevens, P. S.; Iyengar, S. S. The Influence of Water on Anharmonicity, Stability and Vibrational Energy Distribution of Hydrogen-Bonded Adducts in Atmospheric Reactions: Case Study of the OH + Isoprene Reaction Intermediate Using *Ab-Initio* Molecular Dynamics. *J. Phys. Chem. A* **2012**, *116*, 399.
- (13) Hammerich, A. D.; Finlayson-Pitts, B. J.; Gerber, R. B. NOx Reactions on Aqueous Surfaces with Gaseous HCl: Formation of a Potential Precursor to Atmospheric Cl Atoms. *J. Phys. Chem. Lett.* **2012**, *3*, 3405–3410.
- (14) Head-Gordon, M.; Pople, J. A.; Frisch, M. J. MP2 energy evaluation by direct methods. *Chem. Phys. Lett.* **1988**, *153*, 503.
- (15) Schlegel, H. B.; Frisch, M. J. Computational bottlenecks in molecular orbital calculations. In *Theoretical and Computational Models for Organic Chemistry*; Springer, 1991; pp 5–33.

- (16) Christiansen, O.; Koch, H.; Jørgensen, P. The 2nd-Order Approximate Coupled-Cluster Singles and Doubles Model CC2. *Chem. Phys. Lett.* **1995**, 243, 409.
- (17) Ayala, P. Y.; Scuseria, G. E. Linear scaling second-order Moller — Plesset theory in the atomic orbital basis for large molecular systems. *J. Chem. Phys.* **1999**, *110*, 3660—3671.
- (18) Schütz, M.; Hetzer, G.; Werner, H.-J. Low-order scaling local electron correlation methods. I. Linear scaling local MP2. *J. Chem. Phys.* **1999**, *111*, 5691–5705.
- (19) Distasio, R. A.; Steele, R. P.; Rhee, Y. M.; Shao, Y.; Head-Gordon, M. An improved algorithm for analytical gradient evaluation in resolution-of-the-identity second-order Møller-Plesset perturbation theory: Application to alanine tetrapeptide conformational analysis. *J. Comput. Chem.* **2007**, *28*, 839–856.
- (20) Pavošević, F.; Pinski, P.; Riplinger, C.; Neese, F.; Valeev, E. F. SparseMaps—A systematic infrastructure for reduced-scaling electronic structure methods. IV. Linear-scaling second-order explicitly correlated energy with pair natural orbitals. *J. Chem. Phys.* **2016**, *144*, 144109
- (21) Sode, O.; Hirata, S. Second-order many-body perturbation study of solid hydrogen fluoride under pressure. *Phys. Chem. Chem. Phys.* **2012**, *14*, 7765–7779.
- (22) Kumar, A.; Iyengar, S. S. Fragment-based electronic structure for potential energy surfaces using a superposition of fragmentation topologies. *J. Chem. Theory Comput.* **2019**, *15*, 5769.
- (23) Kumar, A.; DeGregorio, N.; Iyengar, S. S. Graph-Theory-Based Molecular Fragmentation for Efficient and Accurate Potential Surface Calculations in Multiple Dimensions. *J. Chem. Theory Comput.* **2021**, 17, 6671–6690.
- (24) Sumner, I.; Iyengar, S. S. Quantum Wavepacket *Ab Initio* Molecular Dynamics: An Approach for Computing Dynamically Averaged Vibrational Spectra Including Critical Nuclear Quantum Effects. *J. Phys. Chem. A* **2007**, *111*, 10313.
- (25) Aleksandrowicz, G.; Alexander, T.; Barkoutsos, P.; Bello, L.; Ben-Haim, Y.; Bucher, D.; Cabrera-Hernández, F. J.; Carballo-Franquis, J.; Chen, A.; Chen, C.-F.; Chow, J. M.; Córcoles-Gonzales, A. D.; Cross, A. J.; Cross, A.; Cruz-Benito, J.; Culver, C.; González, S. D. L. P.; Torre, E. D. L.; Ding, D.; Dumitrescu, E.; Duran, I.; Eendebak, P.; Everitt, M.; Sertage, I. F.; Frisch, A.; Fuhrer, A.; Gambetta, J.; Gago, B. G.; Gomez-Mosquera, J.; Greenberg, D.; Hamamura, I.; Havlicek, V.; Hellmers, J.; Herok, Ł.; Horii, H.; Hu, S.; Imamichi, T.; Itoko, T.; Javadi-Abhari, A.; Kanazawa, N.; Karazeev, A.; Krsulich, K.; Liu, P.; Luh, Y.; Maeng, Y.; Marques, M.; Martín-Fernández, F. J.; McClure, D. T.; McKay, D.; Meesala, S.; Mezzacapo, A.; Moll, N.; Rodríguez, D. M.; Nannicini, G.; Nation, P.; Ollitrault, P.; O'Riordan, L. J.; Paik, H.; Pérez, J.; Phan, A.; Pistoia, M.; Prutyanov, V.; Reuter, M.; Rice, J.; Davila, A. R.; Rudy, R. H. P.; Ryu, M.; Sathaye, N.; Schnabel, C.; Schoute, E.; Setia, K.; Shi, Y.; Silva, A.; Siraichi, Y.; Sivarajah, S.; Smolin, J. A.; Soeken, M.; Takahashi, H.; Tavernelli, I.; Taylor, C.; Taylour, P.; Trabing, K.; Treinish, M.; Turner, W.; Vogt-Lee, D.; Vuillot, C.; Wildstrom, J. A.; Wilson, J.; Winston, E.; Wood, C.; Wood, S.; Wörner, S.; Akhalwaya, I. Y.; Zoufal, C. Qiskit: An Open-source Framework for Quantum Computing. 2019, https://doi.org/10.5281/zenodo.2562111 (accessed September 2021).
- (26) Porras, D.; Cirac, J. I. Effective quantum spin systems with trapped ions. *Phys. Rev. Lett.* **2004**, 92, 207901.
- (27) Richerme, P.; Gong, Z.-X.; Lee, A.; Senko, C.; Smith, J.; Foss-Feig, M.; Michalakis, S.; Gorshkov, A. V.; Monroe, C. Non-local propagation of correlations in quantum systems with long-range interactions. *Nature* **2014**, *511*, 198.
- (28) Cirac, J. I.; Zoller, P. Quantum Computations with Cold Trapped Ions. *Phys. Rev. Lett.* **1995**, *74*, 4091–4094.
- (29) Richerme, P. Two-dimensional ion crystals in radio-frequency traps for quantum simulation. *Phys. Rev. A* **2016**, *94*, 032320.
- (30) Barends, R.; Kelly, J.; Megrant, A.; Veitia, A.; Sank, D.; Jeffrey, E.; White, T. C.; Mutus, J.; Fowler, A. G.; Campbell, B.; Chen, Y.; Chen, Z.; Chiaro, B.; Dunsworth, A.; Neill, C.; O'Malley, P.; Roushan, P.; Vainsencher, A.; Wenner, J.; Korotkov, A. N.; Cleland, A. N.; Martinis,

- J. M. Superconducting quantum circuits at the surface code threshold for faulttolerance tolerance. *Nature* **2014**, *508*, 500–503.
- (31) Barends, R.; Lamata, L.; Kelly, J.; García-Álvarez, L.; Fowler, A.; Megrant, A.; Jeffrey, E.; White, T.; Sank, D.; Mutus, J. Digital quantum simulation of fermionic models with a superconducting circuit. *Nat. Commun.* **2015**, *6*, 7654.
- (32) Lanyon, B. P.; Whitfield, J. D.; Gillett, G. G.; Goggin, M. E.; Almeida, M. P.; Kassal, I.; Biamonte, J. D.; Mohseni, M.; Powell, B. J.; Barbieri, M.; Aspuru-Guzik, A.; White, A. G. Towards quantum chemistry on a quantum computer. *Nat. Chem.* **2010**, *2*, 106–111.
- (33) Aspuru-Guzik, A.; Walther, P. Photonic quantum simulators. *Nat. Phys.* **2012**, *8*, 285–291.
- (34) Knill, E.; Laflamme, R.; Milburn, G. J. A scheme for efficient quantum computation with linear optics. *Nature* **2001**, *409*, 46–52.
- (35) Pellizzari, T.; Gardiner, S. A.; Cirac, J. I.; Zoller, P. Decoherence, continuous observation, and quantum computing: A cavity QED model. *Phys. Rev. Lett.* **1995**, *75*, 3788.
- (36) Loss, D.; DiVincenzo, D. P. Quantum computation with quantum dots. *Phys. Rev. A: At., Mol., Opt. Phys.* **1998**, *57*, 120.
- (37) Imamoglu, A.; Awschalom, D. D.; Burkard, G.; DiVincenzo, D. P.; Loss, D.; Sherwin, M.; Small, A. Quantum information processing using quantum dot spins and cavity QED. *Phys. Rev. Lett.* **1999**, *83*, 4204.
- (38) Calarco, T.; Datta, A.; Fedichev, P.; Pazy, E.; Zoller, P. Spin-based all-optical quantum computation with quantum dots: Understanding and suppressing decoherence. *Phys. Rev. A: At., Mol., Opt. Phys.* **2003**, *68*, 012310.
- (39) Saffman, M.; Walker, T. G.; Mølmer, K. Quantum information with Rydberg atoms. *Rev. Mod. Phys.* **2010**, 82, 2313.
- (40) Saffman, M. Quantum computing with atomic qubits and Rydberg interactions: progress and challenges. *J. Phys. B: At., Mol. Opt. Phys.* **2016**, 49, 202001.
- (41) Bernien, H.; Schwartz, S.; Keesling, A.; Levine, H.; Omran, A.; Pichler, H.; Choi, S.; Zibrov, A. S.; Endres, M.; Greiner, M.; Vuletić, V.; Lukin, M. D. Probing many-body dynamics on a \$1-atom quantum simulator. *Nature* **2017**, *551*, 579–584.
- (42) O'Malley, P. J. J.; Babbush, R.; Kivlichan, I. D.; Romero, J.; McClean, J. R.; Barends, R.; Kelly, J.; Roushan, P.; Tranter, A.; Ding, N.; Campbell, B.; Chen, Y.; Chen, Z.; Chiaro, B.; Dunsworth, A.; Fowler, A. G.; Jeffrey, E.; Lucero, E.; Megrant, A.; Mutus, J. Y.; Neeley, M.; Neill, C.; Quintana, C.; Sank, D.; Vainsencher, A.; Wenner, J.; White, T. C.; Coveney, P. V.; Love, P. J.; Neven, H.; Aspuru-Guzik, A.; Martinis, J. M. Scalable Quantum Simulation of Molecular Energies. *Phys. Rev. X* 2016, 6, 031007.
- (43) Kandala, A.; Mezzacapo, A.; Temme, K.; Takita, M.; Brink, M.; Chow, J. M.; Gambetta, J. M. Hardware-efficient variational quantum eigensolver for small molecules and quantum magnets. *Nature* **2017**, 549, 242.
- (44) Xia, R.; Kais, S. Quantum machine learning for electronic structure calculations. *Nat. Commun.* **2018**, *9*, 4195.
- (45) Gorman, D. J.; Hemmerling, B.; Megidish, E.; Moeller, S. A.; Schindler, P.; Sarovar, M.; Haeffner, H. Engineering vibrationally assisted energy transfer in a trapped-ion quantum simulator. *Phys. Rev. X* **2018**, *8*, 011038.
- (46) Nam, Y.; Chen, J.-S.; Pisenti, N. C.; Wright, K.; Delaney, C.; Maslov, D.; Brown, K. R.; Allen, S.; Amini, J. M.; Apisdorf, J.; Beck, K. M.; Blinov, A.; Chaplin, V.; Chmielewski, M.; Collins, C.; Debnath, S.; Hudek, K. M.; Ducore, A. M.; Keesan, M.; Kreikemeier, S. M.; Mizrahi, J.; Solomon, P.; Williams, M.; Wong-Campos, J. D.; Moehring, D.; Monroe, C.; Kim, J. Ground-state energy estimation of the water molecule on a trapped ion quantum computer. *npj Quantum Inf.* 2020, 6, 33.
- (47) Wang, B.-X.; Tao, M.-J.; Ai, Q.; Xin, T.; Lambert, N.; Ruan, D.; Cheng, Y.-C.; Nori, F.; Deng, F.-G.; Long, G.-L. Efficient quantum simulation of photosynthetic light harvesting. *npj Quantum Inf.* **2018**, *4*, 52.
- (48) Chin, A. W.; Mangaud, E.; Atabek, O.; Desouter-Lecomte, M. Coherent quantum dynamics launched by incoherent relaxation in a

- quantum circuit simulator of a light-harvesting complex. Phys. Rev. A 2018, 97, 063823.
- (49) Potočnik, A.; Bargerbos, A.; Schroder, F. A. Y. N.; Khan, S. A.; Collodo, M. C.; Gasparinetti, S.; Salathe, Y.; Creatore, C.; Eichler, C.; Tureci, H. E.; Chin, A. W.; Wallraff, A. Studying light-harvesting models with superconducting circuits. *Nat. Commun.* **2018**, *9*, 904.
- (50) Peruzzo, A.; McClean, J.; Shadbolt, P.; Yung, M.-H.; Zhou, X.-Q.; Love, P. J.; Aspuru-Guzik, A.; O'Brien, J. L. A variational eigenvalue solver on a photonic quantum processor. *Nat. Commun.* **2014**, *5*, 4213.
- (51) Grimsley, H. R.; Economou, S. E.; Barnes, E.; Mayhall, N. J. An adaptive variational algorithm for exact molecular simulations on a quantum computer. *Nat. Commun.* **2019**, *10*, 3007.
- (52) Arute, F.; Arya, K.; Babbush, R.; Bacon, D.; Bardin, J. C.; Barends, R.; Boixo, S.; Broughton, M.; Buckley, B. B.; Buell, D. A.; Burkett, B.; Bushnell, N.; Chen, Y.; Chen, Z.; Chiaro, B.; Collins, R.; Courtney, W.; Demura, S.; Dunsworth, A.; Farhi, E.; Fowler, A.; Foxen, B.; Gidney, C.; Giustina, M.; Graff, R.; Habegger, S.; Harrigan, M. P.; Ho, A.; Hong, S.; Huang, T.; Huggins, W. J.; Ioffe, L.; Isakov, S. V.; Jeffrey, E.; Jiang, Z.; Jones, C.; Kafri, D.; Kechedzhi, K.; Kelly, J.; Kim, S.; Klimov, P. V.; Korotkov, A.; Kostritsa, F.; Landhuis, D.; Laptev, P.; Lindmark, M.; Lucero, E.; Martin, O.; Martinis, J. M.; McClean, J. R.; McEwen, M.; Megrant, A.; Mi, X.; Mohseni, M.; Mruczkiewicz, W.; Mutus, J.; Naaman, O.; Neeley, M.; Neill, C.; Neven, H.; Niu, M. Y.; O'Brien, T. E.; Ostby, E.; Petukhov, A.; Putterman, H.; Quintana, C.; Roushan, P.; Rubin, N. C.; Sank, D.; Satzinger, K. J.; Smelyanskiy, V.; Strain, D.; Sung, K. J.; Szalay, M.; Takeshita, T. Y.; Vainsencher, A.; White, T.; Wiebe, N.; Yao, Z. J.; Yeh, P.; Zalcman, A. Hartree-Fock on a superconducting qubit quantum computer. Science 2020, 369, 1084-1089.
- (53) Parrish, R. M.; Hohenstein, E. G.; McMahon, P. L.; Martínez, T. J. Quantum Computation of Electronic Transitions Using a Variational Quantum Eigensolver. *Phys. Rev. Lett.* **2019**, *122*, 230401.
- (54) Tkachenko, N. V.; Sud, J.; Zhang, Y.; Tretiak, S.; Anisimov, P. M.; Arrasmith, A. T.; Coles, P. J.; Cincio, L.; Dub, P. A. Correlation-Informed Permutation of Qubits for Reducing Ansatz Depth in the Variational Quantum Eigensolver. *PRX Quantum* **2021**, *2*, 020337.
- (55) Cervera-Lierta, A.; Kottmann, J. S.; Aspuru-Guzik, A. Meta-Variational Quantum Eigensolver: Learning Energy Profiles of Parameterized Hamiltonians for Quantum Simulation. *PRX Quantum* **2021**, *2*, 020329.
- (56) Huggins, W. J.; McClean, J. R.; Rubin, N. C.; Jiang, Z.; Wiebe, N.; Whaley, K. B.; Babbush, R. Efficient and noise resilient measurements for quantum chemistry on near-term quantum computers. *npj Quantum Inf.* **2021**, *7*, 23.
- (57) McClean, J. R.; Rubin, N. C.; Sung, K. J.; Kivlichan, I. D.; Bonet-Monroig, X.; Cao, Y.; Dai, C.; Fried, E. S.; Gidney, C.; Gimby, B. OpenFermion: the electronic structure package for quantum computers. *Quantum Sci. Technol.* **2020**, *5*, 034014.
- (58) Motta, M.; Gujarati, T. P.; Rice, J. E.; Kumar, A.; Masteran, C.; Latone, J. A.; Lee, E.; Valeev, E. F.; Takeshita, T. Y. Quantum simulation of electronic structure with a transcorrelated Hamiltonian: improved accuracy with a smaller footprint on the quantum computer. *Phys. Chem. Chem. Phys.* **2020**, 22, 24270–24281.
- (59) Lang, R. A.; Ryabinkin, I. G.; Izmaylov, A. F. Unitary Transformation of the Electronic Hamiltonian with an Exact Quadratic Truncation of the Baker-Campbell-Hausdorff Expansion. *J. Chem. Theory Comput.* **2021**, *17*, 66–78.
- (60) Ryabinkin, I. G.; Yen, T.-C.; Genin, S. N.; Izmaylov, A. F. Qubit Coupled Cluster Method: A Systematic Approach to Quantum Chemistry on a Quantum Computer. *J. Chem. Theory Comput.* **2018**, 14, 6317–6326.
- (61) Izmaylov, A. F.; Yen, T.-C.; Lang, R. A.; Verteletskyi, V. Unitary Partitioning Approach to the Measurement Problem in the Variational Quantum Eigensolver Method. *J. Chem. Theory Comput.* **2020**, *16*, 190–195.
- (62) Kirby, W. M.; Love, P. J. Variational Quantum Eigensolvers for Sparse Hamiltonians. *Phys. Rev. Lett.* **2021**, *127*, 110503.
- (63) Cervera-Lierta, A.; Kottmann, J. S.; Aspuru-Guzik, A. Meta-Variational Quantum Eigensolver: Learning Energy Profiles of

- Parameterized Hamiltonians for Quantum Simulation. PRX Quantum 2021, 2, 020329.
- (64) Kassal, I.; Jordan, S. P.; Love, P. J.; Mohseni, M.; Aspuru-Guzik, A. Polynomial-time quantum algorithm for the simulation of chemical dynamics. *Proc. Natl. Acad. Sci. U.S.A.* **2008**, *105*, 18681–18686.
- (65) MacDonell, R. J.; Dickerson, C. E.; Birch, C. J. T.; Kumar, A.; Edmunds, C. L.; Biercuk, M. J.; Hempel, C.; Kassal, I. Analog Quantum Simulation of Chemical Dynamics. *Chem. Sci.* **2021**, *12*, 9794–9805.
- (66) Ollitrault, P. J.; Baiardi, A.; Reiher, M.; Tavernelli, I. Hardware efficient quantum algorithms for vibrational structure calculations. *Chem. Sci.* **2020**, *11*, 6842–6855.
- (67) Sawaya, N. P.; Menke, T.; Kyaw, T. H.; Johri, S.; Aspuru-Guzik, A.; Guerreschi, G. G. Resource-efficient digital quantum simulation of d-level systems for photonic, vibrational, and spin-s Hamiltonians. *npj Quantum Inf.* **2020**, *6*, 49.
- (68) Teplukhin, A.; Kendrick, B. K.; Babikov, D. Solving complex eigenvalue problems on a quantum annealer with applications to quantum scattering resonances. *Phys. Chem. Chem. Phys.* **2020**, 22, 26136–26144.
- (69) Jahangiri, S.; Arrazola, J. M.; Quesada, N.; Delgado, A. Quantum algorithm for simulating molecular vibrational excitations. *Phys. Chem. Phys.* **2020**, *22*, 25528–25537.
- (70) Wang, C. S.; Curtis, J. C.; Lester, B. J.; Zhang, Y.; Gao, Y. Y.; Freeze, J.; Batista, V. S.; Vaccaro, P. H.; Chuang, I. L.; Frunzio, L.; Jiang, L.; Girvin, S. M.; Schoelkopf, R. J. Efficient Multiphoton Sampling of Molecular Vibronic Spectra on a Superconducting Bosonic Processor. *Phys. Rev. X* **2020**, *10*, 021060.
- (71) Saha, D.; Iyengar, S. S.; Richerme, P.; Smith, J. M.; Sabry, A. Mapping Quantum Chemical Dynamics Problems to Spin-Lattice Simulators. *J. Chem. Theory Comput.* **2021**, *17*, 6713–6732.
- (72) Nam, Y.; Chen, J.-S.; Pisenti, N. C.; Wright, K.; Delaney, C.; Maslov, D.; Brown, K. R.; Allen, S.; Amini, J. M.; Apisdorf, J.; Beck, K. M.; Blinov, A.; Chaplin, V.; Chmielewski, M.; Collins, C.; Debnath, S.; Hudek, K. M.; Ducore, A. M.; Keesan, M.; Kreikemeier, S. M.; Mizrahi, J.; Solomon, P.; Williams, M.; Wong-Campos, J. D.; Moehring, D.; Monroe, C.; Kim, J. Ground-state energy estimation of the water molecule on a trapped-ion quantum computer. *npj Quantum Inf.* 2020, 6, 33.
- (73) Kandala, A.; Wei, K. X.; Srinivasan, S.; Magesan, E.; Carnevale, S.; Keefe, G. A.; Klaus, D.; Dial, O.; McKay, D. C. Demonstration of a High-Fidelity cnot Gate for Fixed-Frequency Transmons with Engineered ZZ Suppression. *Phys. Rev. Lett.* **2021**, 127, 130501.
- (74) Frisch, M. J.; Trucks, G. W.; Schlegel, H. B.; Scuseria, G. E.; Robb, M. A.; Cheeseman, J. R.; Scalmani, G.; Barone, V.; Petersson, G. A.; Nakatsuji, H.; Li, X.; Caricato, M.; Marenich, A. V.; Bloino, J.; Janesko, B. G.; Gomperts, R.; Mennucci, B.; Hratchian, H. P.; Ortiz, J. V.; Izmaylov, A. F.; Sonnenberg, J. L.; Williams-Young, D.; Ding, F.; Lipparini, F.; Egidi, F.; Goings, J.; Peng, B.; Petrone, A.; Henderson, T.; Ranasinghe, D.; Zakrzewski, V. G.; Gao, J.; Rega, N.; Zheng, G.; Liang, W.; Hada, M.; Ehara, M.; Toyota, K.; Fukuda, R.; Hasegawa, J.; Ishida, M.; Nakajima, T.; Honda, Y.; Kitao, O.; Nakai, H.; Vreven, T.; Throssell, K.; Montgomery, J. A., Jr.; Peralta, J. E.; Ogliaro, F.; Bearpark, M. J.; Heyd, J. J.; Brothers, E. N.; Kudin, K. N.; Staroverov, V. N.; Keith, T. A.; Kobayashi, R.; Normand, J.; Raghavachari, K.; Rendell, A. P.; Burant, J. C.; Iyengar, S. S.; Tomasi, J.; Cossi, M.; Millam, J. M.; Klene, M.; Adamo, C.; Cammi, R.; Ochterski, J. W.; Martin, R. L.; Morokuma, K.; Farkas, O.; Foresman, J. B.; Fox, D. J. Gaussian 16, Revision B.01; Gaussian Inc.: Wallingford CT, 2016.
- (75) Parrish, R. M.; Burns, L. A.; Smith, D. G. A.; Simmonett, A. C.; DePrince, A. E., III; Hohenstein, E. G.; Bozkaya, U.; Sokolov, A. Y.; Di Remigio, R.; Richard, R. M.; Gonthier, J. F.; James, A. M.; McAlexander, H. R.; Kumar, A.; Saitow, M.; Wang, X.; Pritchard, B. P.; Verma, P.; Schaefer, H. F., III; Patkowski, K.; King, R. A.; Valeev, E. F.; Evangelista, F. A.; Turney, J. M.; Crawford, T. D.; Sherrill, C. D. PSI4 1.1: An Open-Source Electronic Structure Program Emphasizing Automation, Advanced Libraries, and Interoperability. *J. Chem. Theory Comput.* 2017, 13, 3185.
- (76) Neese, F. The ORCA program system. Wiley Interdiscip. Rev.: Comput. Mol. Sci. 2012, 2, 73.

- (77) Giannozzi, P.; Baroni, S.; Bonini, N.; Calandra, M.; Car, R.; Cavazzoni, C.; Ceresoli, D.; Chiarotti, G. L.; Cococcioni, M.; Dabo, I.; Dal Corso, A.; de Gironcoli, S.; Fabris, S.; Fratesi, G.; Gebauer, R.; Gerstmann, U.; Gougoussis, C.; Kokalj, A.; Lazzeri, M.; Martin-Samos, L.; Marzari, N.; Mauri, F.; Mazzarello, R.; Paolini, S.; Pasquarello, A.; Paulatto, L.; Sbraccia, C.; Scandolo, S.; Sclauzero, G.; Seitsonen, A. P.; Smogunov, A.; Umari, P.; Wentzcovitch, R. M. QUANTUM ESPRESSO: a modular and open-source software project for quantum simulations of materials. *J. Phys.: Condens. Matter* 2009, 21, 395502.
- (78) Li, J.; Iyengar, S. S. Ab initio Molecular Dynamics using Recursive, Spatially Separated, Overlapping Model Subsystems Mixed Within an ONIOM Based Fragmentation Energy Extrapolation Technique. J. Chem. Theory Comput. 2015, 11, 3978.
- (79) Li, J.; Haycraft, C.; Iyengar, S. S. Hybrid extended Lagrangian, post-Hartree-Fock Born-Oppenheimer ab initio molecular dynamics using fragment-based electronic structure. *J. Chem. Theory Comput.* **2016**, *12*, 2493.
- (80) Haycraft, C.; Li, J.; Iyengar, S. S. Efficient, "On-the-Fly", Born—Oppenheimer and Car—Parrinello-type Dynamics with Coupled Cluster Accuracy through Fragment Based Electronic Structure. *J. Chem. Theory Comput.* **2017**, *13*, 1887.
- (81) Ricard, T. C.; Haycraft, C.; Iyengar, S. S. Adaptive, geometric networks for efficient coarse-grained *ab initio* molecular dynamics with post-Hartree-Fock accuracy. *J. Chem. Theory Comput.* **2018**, *14*, 2852.
- (82) Ricard, T. C.; Iyengar, S. S. Efficiently capturing weak interactions in *ab initio* molecular dynamics through "on-the-fly" basis set extrapolation. *J. Chem. Theory Comput.* **2018**, *14*, 5535.
- (83) Ricard, T. C.; Iyengar, S. S. An efficient and accurate approach to estimate hybrid functional and large basis set contributions to condensed phase systems and molecule-surface interactions. *J. Chem. Theory Comput.* **2020**, *16*, 4790.
- (84) Ricard, T. C.; Kumar, A.; Iyengar, S. S. Embedded, graph-theoretically defined many-body approximations for wavefunction-in-DFT and DFT-in-DFT: applications to gas- and condensed-phase AIMD, and potential surfaces for quantum nuclear effects. *Int. J. Quantum Chem.* **2020**, *120*, No. e26244.
- (85) Zhang, J. H.; Ricard, T. C.; Haycraft, C.; Iyengar, S. S. Weighted-Graph-Theoretic Methods for Many-Body Corrections within ONIOM: Smooth AIMD and the Role of High-Order Many-Body Terms. J. Chem. Theory Comput. 2021, 17, 2672–2690.
- (86) Maseras, F.; Morokuma, K. IMOMM: A new integrated ab initio + molecular mechanics geometry optimization scheme of equilibrium structures and transition states. *J. Comput. Chem.* **1995**, *16*, 1170.
- (87) Zhang, D.-B.; Yuan, Z.-H.; Yin, T. Variational Quantum Eigensolvers by Variance Minimization. **2020**, arXiv:2006.15781. arXiv preprint.
- (88) Ozaki, T.; Kino, H.; Yu, J.; Han, M.; Ohfuchi, M.; Ishii, F.; Sawada, K.; Ohwaki, T.; Weng, H.; Toyoda, M.; Okuno, Y.; Perez, R.; Bell, P.; Duy, T. V. T.; Xiao, Y.; Ito, A.; Terakura, K. *User's Manual of OpenMX*, Ver. 3.8, 2016.
- (89) Björklund, A.; Husfeldt, T.; Koivisto, M. Set partitioning via inclusion-exclusion. SIAM J. Comput. 2009, 39, 546.
- (90) Preskill, J. Quantum Computing in the NISQ era and beyond. *Quantum* **2018**, 2, 79.
- (91) Chia, N.-H.; Chung, K.-M.; Lai, C.-Y. On the Need for Large Quantum Depth. *Proceedings of the 52nd Annual ACM SIGACT Symposium on Theory of Computing, STOC 2020*; Association for Computing Machinery: New York, NY, USA, 2020; pp 902–915.
- (92) Dillon, A. C.; Jones, K. M.; Bekkedahl, T. A.; Kiang, C. H.; Bethune, D. S.; Heben, M. J. Storage of hydrogen in single-walled carbon nanotubes. *Nature* **1997**, *386*, 377–379.
- (93) Chambers, A.; Park, C.; Baker, R. T. K.; Rodriguez, N. M. Hydrogen storage in graphite nanofibers. *J. Phys. Chem. B* **1998**, *102*, 4253–4256.
- (94) Dalebrook, A. F.; Gan, W.; Grasemann, M.; Moret, S.; Laurenczy, G. Hydrogen storage: beyond conventional methods. *Chem. Commun.* **2013**, *49*, 8735–8751.

- (95) Niaz, S.; Manzoor, T.; Pandith, A. H. Hydrogen storage: Materials, methods and perspectives. *Renewable Sustainable Energy Rev.* **2015**, *50*, 457–469.
- (96) Ren, J.; Musyoka, N. M.; Langmi, H. W.; Mathe, M.; Liao, S. Current research trends and perspectives on materials-based hydrogen storage solutions: A critical review. *Int. J. Hydrogen Energy* **2017**, *42*, 289–311.
- (97) Gupta, A.; Baron, G. V.; Perreault, P.; Lenaerts, S.; Ciocarlan, R.-G.; Cool, P.; Mileo, P. G. M.; Rogge, S.; Van Speybroeck, V.; Watson, G.; Van der Voort, P.; Houlleberghs, M.; Breynaert, E.; Martens, J.; Denayer, J. F. M. Hydrogen Clathrates: Next Generation Hydrogen Storage Materials. *Energy Storage Mater.* **2021**, *41*, 69–107.
- (98) Mao, W. L.; Mao, H.-k.; Goncharov, A. F.; Struzhkin, V. V.; Guo, Q.; Hu, J.; Shu, J.; Hemley, R. J.; Somayazulu, M.; Zhao, Y. Hydrogen clusters in clathrate hydrate. *Science* **2002**, *297*, 2247–2249.
- (99) Patchkovskii, S.; Tse, J. S.; Yurchenko, S. N.; Zhechkov, L.; Heine, T.; Seifert, G. Graphene nanostructures as tunable storage media for molecular hydrogen. *Proc. Natl. Acad. Sci. U.S.A.* **2005**, *102*, 10439–10444.
- (100) Granja-DelRío, A.; Alducin, M.; Inaki Juaristi, J.; Lopez, M. J.; Alonso, J. A. Absence of spillover of hydrogen adsorbed on small palladium clusters anchored to graphene vacancies. *Appl. Surf. Sci.* **2021**, *559*, 149835.
- (101) Edwards, P. P.; Kuznetsov, V. L.; David, W. I. F.; Brandon, N. P. Hydrogen and fuel cells: Towards a sustainable energy future. *Energy Policy* **2008**, *36*, 4356–4362.
- (102) Tollefson, J. Hydrogen vehicles: fuel of the future? *Nature News* **2010**, 464, 1262–1264.
- (103) Dodds, P. E.; Staffell, I.; Hawkes, A. D.; Li, F.; Grünewald, P.; McDowall, W.; Ekins, P. Hydrogen and fuel cell technologies for heating: A review. *Int. J. Hydrogen Energy* **2015**, *40*, 2065–2083.
- (104) Xu, M.; Elmatad, Y. S.; Sebastianelli, F.; Moskowitz, J. W.; Bačić, Z. Hydrogen molecule in the small dodecahedral cage of a clathrate hydrate: Quantum five-dimensional calculations of the coupled translation-rotation eigenstates. *J. Phys. Chem. B* **2006**, *110*, 24806—24811
- (105) Turro, N. J.; Martí, A. A.; Chen, J. Y.-C.; Jockusch, S.; Lawler, R. G.; Ruzzi, M.; Sartori, E.; Chuang, S.-C.; Komatsu, K.; Murata, Y. Demonstration of a chemical transformation inside a fullerene. The reversible conversion of the allotropes of H2@ C60. *J. Am. Chem. Soc.* **2008**, *130*, 10506.
- (106) Bacic, Z.; Xu, M.; Felker, P. M. Coupled Translation—Rotation Dynamics of H<sub>2</sub> and H<sub>2</sub>O Inside C60: Rigorous Quantum Treatment. In *Advances in Chemical Physics*; Whaley, K. B., Ed.; Advances in Chemical Physics; Wiley-Blackwell: Commerce Place, 350 Main Street, Malden 02148, MA, USA, 2018; Vol. 163, pp 195–216.
- (107) Tsuge, M.; Namiyoshi, T.; Furuya, K.; Yamazaki, T.; Kouchi, A.; Watanabe, N. Rapid Ortho-to-para Nuclear Spin Conversion of H-2 on a Silicate Dust Surface. *Astrophys. J.* **2021**, *908*, 234.
- (108) Bron, E.; Le Petit, F.; Le Bourlot, J. Efficient ortho-para conversion of H-2 on interstellar grain surfaces. *Astron. Astrophys.* **2016**, 588, A27.
- (109) Bezard, B.; Vinatier, S. On the H-2 abundance and ortho-to-para ratio in Titan's troposphere. *ICARUS 2020, 344, Cassini Science Symposium*; University of Colorado: Boulder, CO, AUG, 2018.
- (110) Lee, S. M.; Park, K. S.; Choi, Y. C.; Park, Y. S.; Bok, J. M.; Bae, D. J.; Nahm, K. S.; Choi, Y. G.; Yu, S. C.; Kim, N.-g.; Frauenheim, T.; Lee, Y. H. Hydrogen adsorption and storage in carbon nanotubes. *Synth. Met.* **2000**, *113*, 209–216.
- (111) Narehood, D.; Kostov, M.; Eklund, P.; Cole, M.; Sokol, P. Deep inelastic neutron scattering of H-2 in single-walled carbon nanotubes. *Phys. Rev. B* **2002**, *65*, 233401.
- (112) Yamaoka, S.; Hyeon-Deuk, K. Distinct molecular dynamics dividing liquid-like and gas-like supercritical hydrogens. *Phys. Chem. Chem. Phys.* **2021**, 23, 22110–22118.
- (113) Deumens, E.; Diz, A.; Longo, R.; Öhrn, Y. Time-Dependent Theoretical Treatments of the Dynamics of Electrons and Nuclei in Molecular-Systems. *Rev. Mod. Phys.* **1994**, *66*, 917.

- (114) Bravyi, S.; Gambetta, J. M.; Mezzacapo, A.; Temme, K. Tapering off qubits to simulate fermionic Hamiltonians. **2017**, arXiv:1701.08213. arXiv preprint.
- (115) Kraft, D. A Software Package for Sequential Quadratic Programming; Wiss. Berichtswesen d. DFVLR Brunswick: Germany, 1988.
- (116) Jordan, P.; Wigner, E. Über das Paulische Äquivalenzverbot. Z. Phys. 1928, 47, 631–651.
- (117) Bravyi, S. B.; Kitaev, A. Y. Fermionic Quantum Computation. *Ann. Phys.* **2002**, 298, 210–226.
- (118) Shen, Y.; Zhang, X.; Zhang, S.; Zhang, J.-N.; Yung, M.-H.; Kim, K. Quantum implementation of the unitary coupled cluster for simulating molecular electronic structure. *Phys. Rev. A* **2017**, *95*, 020501.
- (119) Grimsley, H. R.; Claudino, D.; Economou, S. E.; Barnes, E.; Mayhall, N. J. Is the Trotterized UCCSD Ansatz Chemically Well-Defined? *J. Chem. Theory Comput.* **2019**, *16*, 1–6.
- (120) Smart, S. E.; Mazziotti, D. A. Quantum Solver of Contracted Eigenvalue Equations for Scalable Molecular Simulations on Quantum Computing Devices. *Phys. Rev. Lett.* **2021**, *126*, 070504.